Extension of the Raman behavior-type method to the analysis of polarized-scattering intensities of defects in tetragonal crystals

S. Klauer and M. Wöhlecke
Universität Osnabrück, Fachbereich Physik, Postfach 4469, D-4500 Osnabrück, Federal Republic of Germany
(Received 11 November 1991)

In polarized Raman scattering of point defects in crystals the spectrum is a spatial average of discrete energetically equivalent orientations. Recently, Zhou *et al.* have introduced the behavior-type (BT) method. The primary aim of the BT method is the determination of the defect symmetry O_1 and its vibrational modes, which is reflected in the group-theoretical form of the Raman tensor of the single defect. In cubic systems partial or complete preferential orientation of the defects is often necessary to compete for the loss of information in an ensemble average, in order to yield sufficient discriminating power. In the BT theory an orientating operator $\hat{\mathbf{F}}$ acting on the population numbers of the defects in their discrete orientations is introduced. Instead of solving the set of equations for the polarized Raman intensities for the tensor components, the method focuses on the appearance of symmetry-induced, simple algebraic relations among the so-called Raman *intensity parameters* (IP's), which are characteristic for the possible symmetries of a defect mode. It introduces the concept of the *behavior type* of a mode, which denotes the complete set of IP's, together with the algebraic relations among them. The extension of the BT method to tetragonal crystals necessitates the compilation of the appropriate tables needed for a practical application. The main features of the method introduced by the symmetry of the tetragonal axis can be summarized as follows: (i) The total of 80 possible modes within 25 different symmetry groups O_1 can be classified into 20 sets of representative modes, of which 16 can possibly be distinguished by the method. For comparison in cubic systems there are 124 possible modes in 33 symmetry groups O_1, classified into 24 sets of representative modes, of which 15 can be distinguished. (ii) The optical anisotropy induced by the tetragonal axis reduces the number of possible scattering configurations for polarized light. (iii) The lowered crystal symmetry weakens the averaging effect such that the discriminating power of the method is increased. This holds especially for cases when the defects cannot be orientated, leaving still 13 distinguishable sets of modes compared to only 7 sets in cubic systems. A series of tables essentially contains all the results: In the theoretical part they provide the summary of all possible modes and their classification into sets of representative modes, the influence of preferential orientation, the listing of all possible characteristic BT's, and the relation to the symmetries O_1 of the mode and of the orientating operator $\hat{\mathbf{F}}$ to which the BT's belong. Tables compiled for a practical application provide the relations of the polarized scattering intensities to the IP's, and a guide to select the suitable symmetry of $\hat{\mathbf{F}}$ as well as the discriminating Raman polarization geometries.

I. INTRODUCTION

The properties of dynamical modes of defects in crystals are often investigated by means of infrared absorption or Raman scattering. In both methods the excitation energy of localized elementary excitations is usually more or less well displayed in the spectral distribution. Information on the electronic charge distribution of the point defect is hidden in the polarized spectra. Raman scattering intensities, which depend on the polarization of the incident and scattered light beam, yield information on the defect symmetry and its related local vibrational modes. Recently, a procedure, called the behavior-type (BT) method, has been introduced by Zhou, Goovaerts, and Schoemaker,[1] which allows one to gain important physical insight. This procedure is solely based on symmetry arguments and applicable to randomly or preferentially oriented defects in cubic crystals. The application of the BT method is supported by a set of compiled tables.[1] The use of these tables has been demonstrated for various defects in alkali halides.[2–4]

Although the BT method in its original form has been introduced for nonresonant Raman scattering, under certain favorable circumstances the BT method applies to resonant scattering experiments as well.[5] A full extension to resonant Raman scattering in cubic crystals was proposed in the introductory work already[1] and has been worked out in detail by Leblans.[6] An excellent introduction to the applications of the method for nonresonant and resonant Raman scattering as well as a discussion of the limitation is contained in the review article by Joosen and Schoemaker on applications of the BT method in cubic crystals.[7] Resonant applications include heavy-metal defects with laser-active $Tl^0(1)$ structure, $F_A(Li^+)$ defects in KCl, and electronic Raman scattering of $KCl:Sm^{2+}$.

All studies reported so far had been performed in cubic compounds. An extension of the BT method to tetragonal or even trigonal systems is possible but requires an independent compilation of the corresponding tables and furthermore a discussion of the influence of an optical

axis on the suitable experimental set-ups. Compounds with lower than cubic symmetry are often realized and may occur in a sequence of structural phase transitions. In this contribution we deal with an extension of the BT method for nonresonant scattering to tetragonal crystal structures. In Sec. II the basic ideas of the method shall be outlined. In the next sections the specific features due to the tetragonal symmetry are described and the tables necessary for applications are introduced in some detail, completed by a discussion from both a group-theoretical (Sec. III) and a practical, experimental (Sec. IV) point of view.

II. THE BEHAVIOR-TYPE METHOD FOR TETRAGONAL CRYSTALS

In a crystal containing defects each impurity contributes to the Raman scattering intensity according to the frequency of its local mode and the site symmetry of the polarizability changes with respect to the normal coordinates of the mode. The latter is characterized by the Raman tensor, a second-rank tensor, which is symmetric for nonresonant Raman scattering. The Raman tensor connects the electric fields with polarization vectors $\vec{a}$ and $\vec{b}$ of the incident and scattered lights, respectively. Because each local mode belongs to an irreducible representation of the point group of the defect, nonzero Raman tensor elements or equalities among them are predictable by means of group-theoretical methods for *each* mode. Thus six configurations $(\vec{a}, \vec{b})$ of pairs of electric field orientations are in principle sufficient to determine all tensor elements of a particular mode. Unfortunately, in a scattering experiment focusing on defects in a crystal, an ensemble with different orientations contributes to the signal. Therefore no simple relations can be established between the measured Raman scattering intensities $I_{\vec{a},\vec{v}}$ in the various configurations and the Raman tensor elements of a distinct defect. It is the aim of the BT method to investigate to what extent the defect point group and the irreducible representation of the local mode can be derived from a set of polarized Raman scattering data.

A. Raman scattering intensities and intensity parameters

To allow an easier reading and comparison with the introductory work we use the notation and the terms introduced by Zhou *et al.*[1] The Raman scattering intensity $I_{\vec{a},\vec{b}}$ of an ensemble of point defects in a crystal is the superposition of scattered light $I^{(n)}_{\vec{a},\vec{b}}$ of h energetically equivalent defects with orientations v_n weighed by their population numbers $N^{(n)}$:

$$I_{\vec{a},\vec{b}} = \sum_{n=1}^{h} N^{(n)} I^{(n)}_{\vec{a},\vec{b}}. \tag{1}$$

There are up to h=16 different orientations in tetragonal systems with point group D_{4h}, but because of the invariance of the Raman tensor under spatial inversion, h can be limited to 8. Thus the point group can be restricted to the tetragonal group D_4, which is a subgroup of D_{4h}, when each population number $N^{(n)}$ accounts for the sum of defects in the pairs (v_n, iv_n) of orientations connected by the inversion i. According to Ref. 7 the polarized Raman intensity $I^{(n)}_{\vec{a},\vec{b}}$ of one member of the defect ensemble is given by the following expression:

$$I^{(n)}_{\vec{a},\vec{b}} = kI_0(\vec{a}\overline{\mathbf{T}}^{(n)}\vec{b})^2. \tag{2}$$

Here I_0 denotes the intensity of the incident laser beam and the factor k accounts for the instrumental efficiency governed by the spectrometer, filters, polarizers, and the detector used. The Raman tensor $\overline{\mathbf{T}}^{(n)}$ of the defect in the nth orientation v_n is expressed with respect to the common orthogonal axes of the tetragonal crystal system. Starting with the Raman tensor of one defect in an arbitrary initial orientation v_1, i.e., $\overline{\mathbf{T}}^{(1)}$, all the other $\overline{\mathbf{T}}^{(n)}$ for orientations $v_n = R_n v_1$ follow from $\overline{\mathbf{T}}^{(1)}$ by simple transformations using the h symmetry operations R_n of the crystal point group: $\overline{\mathbf{T}}^{(n)} = R_n \overline{\mathbf{T}}^{(1)} R_n^{-1}$.

The transformed Raman tensors $\overline{\mathbf{T}}^{(n)}$ and the corresponding transformation matrices R_n are given in Table I, expressed in terms of the elements T_{ij} of the Raman tensor $\overline{\mathbf{T}}^{(1)}$ of the mode in its initial orientation v_1, i.e., $T_{ij} = \left(\overline{\mathbf{T}}^{(1)}\right)_{ij}$. The directions α of the rotation axes are expressed in terms of the rectangular frame x, y, z fixed to the principal crystal [100], [010], and [001] directions. For example, $\alpha = x$ means $\alpha \parallel [100]$, $\alpha = \bar{z}$ means $\alpha \parallel [00\bar{1}]$, and $\alpha = x\bar{y}$ means $\alpha \parallel [1\bar{1}0]$.

The intensity $I_{\vec{a},\vec{b}}$, given as a sum over n, is rewritten in a fourfold sum over the components of the corresponding polarization vectors, i.e.,

$$I_{\vec{a},\vec{b}} = \sum_{i,j,k,l=1}^{3} a_i b_j a_k b_l P_{ij\,kl}. \tag{3}$$

The polarization vectors $\vec{a}$ and $\vec{b}$ of the incident and scattered light are expressed in the orthogonal reference frame of the crystal. This defines the components $P_{ij\,kl}$ of a symmetric tensor of rank four:

$$P_{ij\,kl} = kI_0 \sum_{n=1}^{h} N^{(n)} T^{(n)}_{ij} T^{(n)}_{kl}, \tag{4}$$

which are called intensity parameters (IP). From the set of 81 elements $P_{ij\,kl}$ there remain only 21 independent IP, the maximum number of independent elements of a symmetric fourth-rank tensor. It is pointed out that the IP are not simple shortcuts. The introduction of the IP in Eq. (4) provides a separation between merely geometrical factors due to the scattering configuration, which can be externally adjusted in the experiment, and intrinsic properties of the defect ensemble. The $P_{ij\,kl}$ conceal all the information on the population numbers $N^{(n)}$ and on the symmetry of the defect contained in the T_{ij}, which can principally be derived from polarized Raman data.

Experimental constraints, such as the need of set-ups with different scattering configurations for several crys-

TABLE I. The Raman tensors $\overline{\mathbf{T}}^{(n)}$ transformed to the eight possible orientations of a defect in a tetragonal crystal, starting from a defect with a general Raman tensor in an arbitrary initial orientation. The transformation matrices $R_n \in D_4[001]$, $n = 1, \ldots, 8$ are expressed with respect to the fixed crystal system (x, y, z). The $\overline{\mathbf{T}}^{(n)}$ and R_n are given an identifying number for reference.

1: $C_1 = \begin{pmatrix} 1 & & \\ & 1 & \\ & & 1 \end{pmatrix}$	2: $C_2^z = \begin{pmatrix} -1 & & \\ & -1 & \\ & & 1 \end{pmatrix}$	3: $C_2^x = \begin{pmatrix} 1 & & \\ & -1 & \\ & & -1 \end{pmatrix}$	4: $C_2^y = \begin{pmatrix} -1 & & \\ & 1 & \\ & & -1 \end{pmatrix}$
$\begin{pmatrix} T_{11} & T_{12} & T_{13} \\ T_{21} & T_{22} & T_{23} \\ T_{31} & T_{32} & T_{33} \end{pmatrix}$	$\begin{pmatrix} T_{11} & T_{12} & -T_{13} \\ T_{21} & T_{22} & -T_{23} \\ -T_{31} & -T_{32} & T_{33} \end{pmatrix}$	$\begin{pmatrix} T_{11} & -T_{12} & -T_{13} \\ -T_{21} & T_{22} & T_{23} \\ -T_{31} & T_{32} & T_{33} \end{pmatrix}$	$\begin{pmatrix} T_{11} & -T_{12} & T_{13} \\ -T_{21} & T_{22} & -T_{23} \\ T_{31} & -T_{32} & T_{33} \end{pmatrix}$
5: $C_2^{\overline{x}y} = \begin{pmatrix} & -1 & \\ -1 & & \\ & & -1 \end{pmatrix}$	6: $C_2^{xy} = \begin{pmatrix} & 1 & \\ 1 & & \\ & & -1 \end{pmatrix}$	7: $C_4^z = \begin{pmatrix} & -1 & \\ 1 & & \\ & & 1 \end{pmatrix}$	8: $C_4^{\overline{z}} = \begin{pmatrix} & 1 & \\ -1 & & \\ & & 1 \end{pmatrix}$
$\begin{pmatrix} T_{22} & T_{21} & T_{23} \\ T_{12} & T_{11} & T_{13} \\ T_{32} & T_{31} & T_{33} \end{pmatrix}$	$\begin{pmatrix} T_{22} & T_{21} & -T_{23} \\ T_{12} & T_{11} & -T_{13} \\ -T_{32} & -T_{31} & T_{33} \end{pmatrix}$	$\begin{pmatrix} T_{22} & -T_{21} & -T_{23} \\ -T_{12} & T_{11} & T_{13} \\ -T_{32} & T_{31} & T_{33} \end{pmatrix}$	$\begin{pmatrix} T_{22} & -T_{21} & T_{23} \\ -T_{12} & T_{11} & -T_{13} \\ T_{32} & -T_{31} & T_{33} \end{pmatrix}$

tals with high accuracy of the alignment and the polarization dependence of light propagating in crystals with one optical axis, usually impede the determination of all the $P_{ij\,kl}$ from 21 independent scattering configurations. Because the factor k is unknown, relative IP are obtainable only.

For a better survey and easier comparison with previous BT work the shorthand notation introduced in Ref. 1

TABLE II. Explicit expressions for the intensity parameters (IP) of defect ensembles in tetragonal crystals, expressed as a function of the population numbers $N^{(n)}$ and the Raman tensor components $T_{ij} = \left(\overline{\mathbf{T}}^{(1)}\right)_{ij}$ of the mode in its initial orientation.

$$kI_0\,P_{1111} = \mathbf{q_1} = \mathbf{kI_0}(\mathbf{T_{11}^2 M_1 + T_{22}^2 M_2})$$
$$kI_0\,P_{2222} = \mathbf{q_2} = \mathbf{kI_0}(\mathbf{T_{22}^2 M_1 + T_{11}^2 M_2})$$
$$kI_0\,P_{3333} = \mathbf{q_3} = \mathbf{kI_0\,T_{33}^2 M}$$

$$kI_0\,P_{2233} = \mathbf{r_1} = \mathbf{kI_0}(\mathbf{T_{22}T_{33}M_1 + T_{11}T_{33}M_2})$$
$$kI_0\,P_{1133} = \mathbf{r_2} = \mathbf{kI_0}(\mathbf{T_{11}T_{33}M_1 + T_{22}T_{33}M_2})$$
$$kI_0\,P_{1122} = \mathbf{r_3} = \mathbf{kI_0\,T_{11}T_{22}M}$$

$$kI_0\,P_{2323} = \mathbf{s_1} = \mathbf{kI_0}(\mathbf{T_{23}^2 M_1 + T_{13}^2 M_2})$$
$$kI_0\,P_{1313} = \mathbf{s_2} = \mathbf{kI_0}(\mathbf{T_{13}^2 M_1 + T_{23}^2 M_2})$$
$$kI_0\,P_{1212} = \mathbf{s_3} = \mathbf{kI_0\,T_{12}^2 M}$$

$$kI_0\,P_{1213} = \mathbf{t_1} = \mathbf{kI_0}(\mathbf{T_{12}T_{13}M_1' + T_{21}T_{23}M_2'})$$
$$kI_0\,P_{1223} = \mathbf{t_2} = \mathbf{kI_0}(\mathbf{T_{12}T_{23}M_1'' + T_{21}T_{13}M_2''})$$
$$kI_0\,P_{1323} = \mathbf{t_3} = \mathbf{kI_0\,T_{13}T_{23}(M_1''' + M_2''')}$$

$$kI_0\,P_{1123} = \mathbf{u_1} = \mathbf{kI_0}(\mathbf{T_{11}T_{23}M_1' + T_{13}T_{22}M_2'})$$
$$kI_0\,P_{2213} = \mathbf{u_2} = \mathbf{kI_0}(\mathbf{T_{22}T_{13}M_1'' + T_{11}T_{23}M_2''})$$
$$kI_0\,P_{3312} = \mathbf{u_3} = \mathbf{kI_0\,T_{12}T_{33}(M_1''' + M_2''')}$$

$$kI_0\,P_{2223} = \mathbf{v_1} = \mathbf{kI_0}(\mathbf{T_{22}T_{23}M_1' + T_{11}T_{13}M_2'})$$
$$kI_0\,P_{3323} = \mathbf{v_2} = \mathbf{kI_0}(\mathbf{T_{23}T_{33}M_1' + T_{13}T_{33}M_2'})$$
$$kI_0\,P_{1113} = \mathbf{v_3} = \mathbf{kI_0}(\mathbf{T_{11}T_{13}M_1'' + T_{22}T_{23}M_2''})$$
$$kI_0\,P_{3313} = \mathbf{v_4} = \mathbf{kI_0}(\mathbf{T_{13}T_{33}M_1'' + T_{23}T_{33}M_2''})$$
$$kI_0\,P_{1112} = \mathbf{v_5} = \mathbf{kI_0}(\mathbf{T_{11}T_{12}M_1''' + T_{21}T_{22}M_2'''})$$
$$kI_0\,P_{2212} = \mathbf{v_6} = \mathbf{kI_0}(\mathbf{T_{21}T_{22}M_1''' + T_{11}T_{12}M_2'''})$$

With the following abbreviations:

$$M_1 = N_1 + N_2 + N_3 + N_4; \qquad M_2 = N_5 + N_6 + N_7 + N_8; \qquad M = M_1 + M_2;$$
$$M_1' = N_1 - N_2 + N_3 - N_4; \qquad M_2' = N_5 - N_6 + N_7 - N_8;$$
$$M_1'' = N_1 - N_2 - N_3 + N_4; \qquad M_2'' = N_5 - N_6 - N_7 + N_8;$$
$$M_1''' = N_1 + N_2 - N_3 - N_4; \qquad M_2''' = N_5 + N_6 - N_7 - N_8;$$

shall be used to designate the IP:

$$\begin{aligned} q_1 &= kI_0P_{11\,11},\ q_2 = kI_0P_{22\,22},\ q_3 = kI_0P_{33\,33},\\ r_1 &= kI_0P_{22\,33},\ r_2 = kI_0P_{11\,33},\ r_3 = kI_0P_{11\,22},\\ s_1 &= kI_0P_{23\,23},\ s_2 = kI_0P_{13\,13},\ s_3 = kI_0P_{12\,12},\\ t_1 &= kI_0P_{12\,13},\ t_2 = kI_0P_{12\,23},\ t_3 = kI_0P_{13\,23},\\ u_1 &= kI_0P_{11\,23},\ u_2 = kI_0P_{22\,13},\ u_3 = kI_0P_{33\,12},\\ v_1 &= kI_0P_{22\,23},\ v_2 = kI_0P_{33\,23},\ v_3 = kI_0P_{11\,13},\\ v_4 &= kI_0P_{33\,13},\ v_5 = kI_0P_{11\,12},\ v_6 = kI_0P_{22\,12}, \end{aligned} \tag{5}$$

Using Eq. (4) and the tensors in Table I the explicit expressions of Table II for the 21 IP were calculated as a function of the population numbers $N^{(n)}$ and the Raman tensor elements T_{ij}.

From Table II it is easily verified that the IP q_i and s_i are positive or zero, while nothing can be predicted for the other. Similar to the IP, only relative values of the population numbers $N^{(n)}$ and the tensor elements T_{ij} can be determined from Raman data in practice.

Taking into account that only relative values are available, 20 independent equations derived from Eq. (4) correspond to 28 unknowns [5 T_{ij} and $(h-1) = 23N^{(n)}$] in cubic systems. Therefore, the 21 scattering intensities are not sufficient to yield all unknowns. The situation is drastically changed in tetragonal systems. Here the strongly reduced number h=8 of different orientations results in only 12 unknowns to be determined from a set of 20 equations. Unfortunately this advantage can possibly not be fully exploited because of limitations due to the light polarization behavior in uniaxial crystals, see the discussion in Sec. IV. Similar to cubic crystals, the production of an anisotropy in the distribution of the defects onto their orientations will generally allow us to extract information on the symmetry of the mode to higher extent, but will complicate the evaluation of the equations in Table II.

A complete solution of these equations, which are even cubic with respect to the unknowns $\{N^{(n)}, T_{ij}\}$ may become very difficult, if not impossible, due to a lack of sufficient experimental precision. In most cases this is beyond the capability and the aim of an investigation. Usually knowledge of the defect symmetry and the transformation properties (irreducible representations) of the modes allow clear conclusions on the incorporation of a defect.

B. Preferential orientation of the defects

The intensity parameters depend on the population numbers $N^{(n)}$ and the Raman tensors $\overline{\mathbf{T}}^{(\mathbf{n})}$, see Eq. (4). Both are influenced by the symmetry under study. First, the symmetry group O_1 of the defect governs the actual form of the tensor $\overline{\mathbf{T}}^{(\mathbf{1})}$ and therefore also the IP values. Second, the usual initial random population distributions $N^{(n)}$ can be altered by applying external forces. The influence of the forces are described by a so-called orientating operator $\hat{\mathbf{F}}$ acting on the population numbers. The symmetry of $\hat{\mathbf{F}}$ is defined to be the largest subgroup $F_1 \subset D_{4h}$, which leaves $\hat{\mathbf{F}}$ invariant. Orientations related by the inversion i, v_n, and iv_n, may be influenced by $\hat{\mathbf{F}}$ in a different manner, but in the BT method they are treated as partners with one common population number $N^{(n)}$, because the Raman tensor is invariant under inversion. This allows us to treat $\hat{\mathbf{F}}$ in the tetragonal group D_4.

TABLE III. (a) The right cosets of the 9 representative symmetries $F_1 \subset D_4$ of the orientating operator $\hat{\mathbf{F}}$. (b) The left cosets of the defect symmetry group $O_1 \subset D_4$. The orientations are labeled with the numbers of the symmetry elements of the tetragonal group D_4 as introduced in Table I. The subscripts label the different cosets. Orientations, which belong to the same coset, possess the same population numbers.

F_1	(a) The right cosets of F_1
C_1	$\{1\}_1\ \{2\}_2\ \{3\}_3\ \{4\}_4\ \{5\}_5\ \{6\}_6\ \{7\}_7\ \{8\}_8$
$C_2[001]$	$\{1, 2\}_1\ \{3, 4\}_2\ \{5, 6\}_3\ \{7, 8\}_4$
$C_2[100]$	$\{1, 3\}_1\ \{2, 4\}_2\ \{5, 7\}_3\ \{6, 8\}_4$
$C_2[110]$	$\{1, 6\}_1\ \{2, 5\}_2\ \{3, 7\}_3\ \{4, 8\}_4$
$D_2[100]$	$\{1, 2, 3, 4\}_1\ \{5, 6, 7, 8\}_2$
$D_2[110]$	$\{1, 2, 5, 6\}_1\ \{3, 4, 7, 8\}_2$
$C_4[001]$	$\{1, 2, 7, 8\}_1\ \{3, 4, 5, 6\}_2$
$D_4[001]$	$\{1, 2, 3, 4, 5, 6, 7, 8\}_1$

O_1	(b) The left cosets of O_1
C_1	$\{1\}_1\ \{2\}_2\ \{3\}_3\ \{4\}_4\ \{5\}_5\ \{6\}_6\ \{7\}_7\ \{8\}_8$
$C_2[001]$	$\{1, 2\}_1\ \{3, 4\}_2\ \{5, 6\}_3\ \{7, 8\}_4$
$C_2[010]$	$\{1, 4\}_1\ \{2, 3\}_2\ \{5, 7\}_3\ \{6, 8\}_4$
$C_2[110]$	$\{1, 6\}_1\ \{2, 5\}_2\ \{3, 8\}_3\ \{4, 7\}_4$
$D_2[100]$	$\{1, 2, 3, 4\}_1\ \{5, 6, 7, 8\}_2$
$D_2[110]$	$\{1, 2, 5, 6\}_1\ \{3, 4, 7, 8\}_2$
$C_4[001]$	$\{1, 2, 7, 8\}_1\ \{3, 4, 5, 6\}_2$
$D_4[001]$	$\{1, 2, 3, 4, 5, 6, 7, 8\}_1$

Under the action of $\hat{\mathbf{F}}$ there will be subsets of orientations v_n, which are influenced in the same way by the symmetry F_1, thus decomposing the set $\mathbf{V}$ of all orientations into disjunct subsets $V_1, V_2, \ldots, V_\sigma$ of orientations with the same population number. Zhou *et al.*[1] have shown formally, that these subsets correspond to the right cosets $F_1, F_2, \ldots, F_\sigma$ created by the symmetry group F_1. This result allows us to construct the sets of orientations with the same population number given in Table III(a). The possible subgroups $F_1 \subset D_{4h}$, which are considered for the symmetry of the orientating operator $\hat{\mathbf{F}}$ are listed in Table IV, where they are classified into 8 groups of representative symmetries F_1. The sets of independent population numbers are derived from the right cosets of the point group F_1, see Table III(a). The number of independent population numbers equals σ, the number of right cosets. To illustrate the influence of external forces described by $\hat{\mathbf{F}}$, one can say that $\hat{\mathbf{F}}$ arranges those orientations v_n into one coset, which have the same angle with the principal axis of F_1.

TABLE IV. (a) The subgroups $F_1' \subset D_{4h}[001]$ considered for the orientating operator $\hat{\mathbf{F}}$, classified into 8 sets of representative symmetries $F_1 \subset D_4[001]$. Also given are σ, the number of independent population numbers and N_{var}, the maximum number of unknowns. (b) The constraints among the IP induced by the symmetry of F_1 are explicitly given in the short IP notation. Also given is μ_{IP}, the number of obviously independent IP.

F_1	σ	N_{var}	(a) Equivalent subgroups F_1'
C_1	8	12	C_1, S_2
$C_2[001]$	4	8	$C_2[001]$, $C_{1h}[001]$, $C_{2h}[001]$
$C_2[100]$	4	8	$C_2[100]$, $C_{1h}[100]$, $C_{2h}[100]$
$C_2[110]$	4	8	$C_2[110]$, $C_{1h}[110]$, $C_{2h}[110]$
$D_2[100]$	2	6	$D_2[100,010,001]$, $C_{2v}[100](010,001)$, $D_{2h}[100,010,001]$
$D_2[110]$	2	6	$D_2[110,1\bar{1}0,001]$, $C_{2v}[001](110,1\bar{1}0)$, $D_{2h}[110,1\bar{1}0,001]$, $C_{2v}[1\bar{1}0](110,001)$
$C_4[001]$	2	6	$C_4[001]$, $S_4[001]$, $C_{4h}[001]$
$D_4[001]$	1	5	$D_4[001]$, $C_{4v}[001]$, $D_{4h}[001]$, $D_{2d}[100,010,001](110,1\bar{1}0)$, $D_{2d}[110,1\bar{1}0,001](100,010)$

F_1	μ_{IP}	(b) F_1-symmetry imposed constraints	
C_1	20		a
$C_2[001]$	12	$t_1 = t_2 = u_1 = u_2 = v_1 = v_2 = v_3 = v_4 = 0$	a
$C_2[100]$	12	$t_2 = t_3 = u_2 = u_3 = v_3 = v_4 = v_5 = v_6 = 0$	a
$C_2[110]$	11	$q_1 = q_2$, $r_1 = r_2$, $s_1 = s_2$, $t_1 = -t_2$, $u_1 = -u_2$, $v_1 = -v_3$, $v_2 = -v_4$, $v_5 = v_6$	b,c
$D_2[100]$	8	$t_1 = t_2 = t_3 = u_1 = u_2 = u_3 = v_1 = v_2 = v_3 = v_4 = v_5 = v_6 = 0$	a
$D_2[110]$	7	$t_1 = t_2 = u_1 = u_2 = v_1 = v_2 = v_3 = v_4 = 0$, $q_1 = q_2$, $r_1 = r_2$, $s_1 = s_2$, $v_5 = v_6$	b,c
$C_4[001]$	6	$t_1 = t_2 = t_3 = u_1 = u_2 = u_3 = v_1 = v_2 = v_3 = v_4 = 0$, $q_1 = q_2$, $r_1 = r_2$, $s_1 = s_2$, $v_5 = -v_6$	b
$D_4[001]$	5	$t_1 = t_2 = t_3 = u_1 = u_2 = u_3 = v_1 = v_2 = v_3 = v_4 = v_5 = v_6 = 0$, $q_1 = q_2$, $r_1 = r_2$, $s_1 = s_2$	b

[a] $(q_1 + q_2 + 2r_3)^{1/2} = (r_1 + r_2)/(q_3)^{1/2}$.
[b] $(q_1 + r_3)^{1/2} = (2r_1/q_3)^{1/2}$.
[c] $q_3/r_1 = 2u_3/v_5$.

TABLE V. The symmetric Raman tensors for all the possible dynamical local modes which can occur in a tetragonal crystal structure, arranged according to the 25 essentially different possible symmetry groups $O_1' \subset D_{4h}[001]$. The tensors have been transformed from the local frame (x', y', z') of the defect to the reference frame (x, y, z) of the crystal. The directions of the local reference axes are given with respect to the crystal axes $x \parallel [100]$, $y \parallel [010]$, $z \parallel [001]$. The explicit expressions for the tensor elements are given in the footnote[a] of the table.

Defect symmetry O_1 Defect frame	Raman active dynamical modes Raman tensors			
C_1 S_2	$A(x', y', z'; R_{x'}, R_{y'}, R_{z'})$ $A_g(R_{x'}, R_{y'}, R_{z'})$			
$x' \parallel [100]$ $y' \parallel [010]$ $z' \parallel [001]$	$\begin{pmatrix} a_1 & d & f' \\ d & a_2 & f \\ f' & f & a_3 \end{pmatrix}$			
$C_2[010]$ $C_{1h}(010)$ $C_{2h}[010]$	$A(y'; R_{y'})$ $A'(x', z'; R_{y'})$ $A_g(R_{y'})$		$B(x', z'; R_{x'}, R_{z'})$ $A''(y'; R_{x'}, R_{z'})$ $B_g(R_{x'}, R_{z'})$	
$x' \parallel [100]$ $y' \parallel [010]$ $z' \parallel [001]$	$\begin{pmatrix} a_1 & & f' \\ & a_2 & \\ f' & & a_3 \end{pmatrix}$		$\begin{pmatrix} & d & \\ d & & f \\ & f & \end{pmatrix}$	
$C_2[001]$ $C_{1h}(001)$ $C_{2h}[001]$	$A(y'; R_{y'})$ $A'(x', z'; R_{y'})$ $A_g(R_{y'})$		$B(x', z'; R_{x'}, R_{z'})$ $A''(y'; R_{x'}, R_{z'})$ $B_g(R_{x'}, R_{z'})$	
$x' \parallel [100]$ $y' \parallel [001]$ $z' \parallel [0\bar{1}0]$	$\begin{pmatrix} a_1 & -f' & \\ -f' & a_3 & \\ & & a_2 \end{pmatrix}$		$\begin{pmatrix} & & d \\ & & -f \\ d & -f & \end{pmatrix}$	
$C_2[110]$ $C_{1h}(110)$ $C_{2h}[110]$	$A(y'; R_{y'})$ $A'(x', z'; R_{y'})$ $A_g(R_{y'})$		$B(x', z'; R_{x'}, R_{z'})$ $A''(y'; R_{x'}, R_{z'})$ $B_g(R_{x'}, R_{z'})$	
$x' \parallel [1\bar{1}0]$ $y' \parallel [110]$ $z' \parallel [001]$	$\begin{pmatrix} a & -c & \frac{1}{\sqrt{2}}f' \\ -c & a & -\frac{1}{\sqrt{2}}f' \\ \frac{1}{\sqrt{2}}f' & -\frac{1}{\sqrt{2}}f' & a_3 \end{pmatrix}$		$\begin{pmatrix} d & & \frac{1}{\sqrt{2}}f \\ & -d & \frac{1}{\sqrt{2}}f \\ \frac{1}{\sqrt{2}}f & \frac{1}{\sqrt{2}}f & \end{pmatrix}$	
$D_2[100, 010, 001]$ $C_{2v}[001](100, 010)$ $D_{2h}[001, 100, 010]$	A $A_1(z')$ A_g	$B_1(z'; R_{z'})$ $A_2(R_{z'})$ $B_{1g}(R_{z'})$	$B_2(y'; R_{y'})$ $B_1(x'; R_{y'})$ $B_{2g}(R_{y'})$	$B_3(x'; R_{x'})$ $B_2(y'; R_{x'})$ $B_{3g}(R_{x'})$
$x' \parallel [100]$ $y' \parallel [010]$ $z' \parallel [001]$	$\begin{pmatrix} a_1 & & \\ & a_2 & \\ & & a_3 \end{pmatrix}$	$\begin{pmatrix} & d & \\ d & & \end{pmatrix}$	$\begin{pmatrix} & f' & \\ f' & & \end{pmatrix}$	$\begin{pmatrix} & f & \\ f & & \end{pmatrix}$
$D_2[001, 110, 1\bar{1}0]$ $C_{2v}[001](110, 1\bar{1}0)$ $D_{2h}[001, 110, 1\bar{1}0]$	A $A_1(z')$ A_g	$B_1(z'; R_{z'})$ $A_2(R_{z'})$ $B_{1g}(R_{z'})$	$B_2(y'; R_{y'})$ $B_1(x'; R_{y'})$ $B_{2g}(R_{y'})$	$B_3(x'; R_{x'})$ $B_2(y'; R_{x'})$ $B_{3g}(R_{x'})$
$x' \parallel [1\bar{1}0]$ $y' \parallel [110]$ $z' \parallel [001]$	$\begin{pmatrix} a & -c & \\ -c & a & \\ & & a_3 \end{pmatrix}$	$\begin{pmatrix} d & & \\ & -d & \\ & & \end{pmatrix}$	$\frac{1}{\sqrt{2}}\begin{pmatrix} & f' & \\ & & -f' \\ f' & -f' & \end{pmatrix}$	$\frac{1}{\sqrt{2}}\begin{pmatrix} & f & \\ & f & \\ f & f & \end{pmatrix}$
$C_{2v}[1\bar{1}0](110, 001)$	$A_1(z')$	$B_1(x'; R_{y'})$	$B_2(y'; R_{x'})$	$A_2(R_{z'})$
$x' \parallel [110]$ $y' \parallel [001]$ $z' \parallel [1\bar{1}0]$	$\begin{pmatrix} h & -c' & \\ -c' & h & \\ & & a_2 \end{pmatrix}$	$\begin{pmatrix} f' & \\ & -f' \end{pmatrix}$	$\frac{1}{\sqrt{2}}\begin{pmatrix} & f & \\ & & -f \\ f & -f & \end{pmatrix}$	$\frac{1}{\sqrt{2}}\begin{pmatrix} & d & \\ & & d \\ d & d & \end{pmatrix}$

TABLE V. *(Continued).*

Defect symmetry O_1 Defect frame	Raman active dynamical modes Raman tensors				
$C_4[001]$	$A(z';R_{z'})$	B	$E(x';R_{x'})$	$E(y';R_{y'})$	
$S_4[001]$	$A(R_{z'})$	$B(z')$	$E(x';R_{x'})$	$E(y';R_{y'})$	
$C_{4h}[001]$	$A_g(R_{z'})$	B_g	$E_g^{(1)}(R_{x'})$	$E_g^{(2)}(R_{y'})$	
$x' \parallel [100]$ $y' \parallel [010]$ $z' \parallel [001]$	$\begin{pmatrix} a & & \\ & a & \\ & & a_3 \end{pmatrix}$	$\begin{pmatrix} c & d & \\ d & -c & \\ & & \end{pmatrix}$	$\frac{1}{\sqrt{2}}\begin{pmatrix} & & f' \\ & & f \\ f' & f & \end{pmatrix}$	$\frac{1}{\sqrt{2}}\begin{pmatrix} & & -f \\ & & f' \\ -f & f' & \end{pmatrix}$	
$D_4[001, 100, 010, 110, 1\bar{1}0]$	A_1	B_1	B_2	$E(x';R_{x'})$	$E(y';R_{y'})$
$D_{4h}[001, 100, 010, 110, 1\bar{1}0]$	A_{1g}	B_{1g}	B_{2g}	$E_g^{(1)}(R_{x'})$	$E_g^{(2)}(R_{y'})$
$D_{2d}[001, 100, 010](110, 1\bar{1}0)$	A_1	B_1	$B_2(z')$	$E(x', R_{x'})$	$E(y', R_{y'})$
$x' \parallel [100]$ $y' \parallel [010]$ $z' \parallel [001]$	$\begin{pmatrix} a & & \\ & a & \\ & & a_3 \end{pmatrix}$	$\begin{pmatrix} c & & \\ & -c & \\ & & \end{pmatrix}$	$\begin{pmatrix} & d & \\ d & & \\ & & \end{pmatrix}$	$\begin{pmatrix} & & \\ & f & \\ & f & \end{pmatrix}$	$\begin{pmatrix} & & -f \\ & & \\ -f & & \end{pmatrix}$
$C_{4v}[001](100, 010, 110, 1\bar{1}0)$	$A_1(z')$	B_1	B_2	$E(y', R_{x'})$	$E(x', R_{y'})$
$x' \parallel [100]$ $y' \parallel [010]$ $z' \parallel [001]$	$\begin{pmatrix} a & & \\ & a & \\ & & a_3 \end{pmatrix}$	$\begin{pmatrix} c & & \\ & -c & \\ & & \end{pmatrix}$	$\begin{pmatrix} & d & \\ d & & \\ & & \end{pmatrix}$	$\begin{pmatrix} & & \\ & f' & \\ & f' & \end{pmatrix}$	$\begin{pmatrix} & & f' \\ & & \\ f' & & \end{pmatrix}$

[a]The explicit expressions for the symbols in the tensor elements: $a_1 = x'x'$; $a_2 = y'y'$; $a_3 = z'z'$; $a = \frac{1}{2}(x'x' + y'y')$; $c = \frac{1}{2}(x'x' - y'y')$; $d = \frac{1}{2}(x'y' + y'x')$; $f = \frac{1}{2}(y'z' + z'y')$; $f' = \frac{1}{2}(x'z' + z'x')$.

III. IDENTIFICATION OF DYNAMICAL MODES IN TETRAGONAL CRYSTALS BY A RAMAN BEHAVIOR-TYPE ANALYSIS

A. Representative dynamical modes in tetragonal crystals

The Raman tensor of a dynamical mode is determined by the symmetry of the mode and its group-theoretical representation. The symmetry O_1 of a defect mode in a crystal must be a subgroup of the crystallographic point group of the host lattice, $O_1 \subset D_4$. The set of possible local modes in tetragonal crystals are listed in Table V. The corresponding Raman tensors are taken from the tables in Ref. 8.

It is expected, that due to the lower symmetry in tetragonal crystals as compared to cubic systems, less information on the Raman tensor $\overline{\mathbf{T}}^{(1)}$ is lost in Raman experiments. This is true, because the number of energetically equivalent orientations, over which the Raman signal has to be averaged, is reduced from h=24 to 8.

Additionally, the special role of the high symmetric tetragonal axis is expected to prevent parts of the information from being "washed out." This is reflected in the explicit expressions of the IP given in Table II. As a consequence, several independent initial orientations v_1, compatible with the local symmetry O_1, must be taken into account for defects with some special orientation of the principal axis of O_1. In particular, this was necessary for the sets of modes with the following representative symmetries:

$$\{C_2[010], C_2[001], C_2[110]\}, \{D_2[100], D_2[110]\},$$

see Tables V and VI. Especially, as a consequence of the extraordinary role of the fourfold axis, O_1=$C_2[010]$ which is equivalent to $C_2[100]$ leads to different results compared to $C_2[001]$. These cases could not be distinguished in cubic systems.

Similar to the case of defect modes in cubic crystals different possible modes of the same defect point group O_1 cannot be distinguished at all by means of Raman experiments, even if the complete set of the 21 IP is available, see Ref. 1 and the footnote in Ref. 7. This results partly from the explicit forms of the Raman tensors and partly from an internal symmetry in the equations of Table II. Referring to the more complete description of similar observations for the equivalent equations in cubic systems (Appendix D in Ref. 1), this internal symmetry consists in a permutation $\hat{\mathbf{P}}_{12}$ of the indices in the set

$$\mathbf{X} = \{T_{11}, T_{22}, T_{33}, T_{23}, T_{13}, T_{12}, M_1, M_2, M_1', M_2', M_1'', M_2'', M_1''', M_2'''\},$$

of unknowns in the equations of Table II, which leaves them invariant:

$$\hat{\mathbf{P}}_{12}\mathbf{X} \equiv \{T_{22}, T_{11}, T_{33}, T_{13}, T_{23}, T_{12}, M_2, M_1, M_2', M_1', M_2'', M_1'', M_2''', M_1'''\}.$$

The indices of $\hat{\mathbf{P}}$ refer to the indices of the Raman tensor elements to be permuted. As a consequence of this, the following modes cannot be distinguished. (i) The B_2 and B_3 modes of a defect with symmetry $O_1{=}D_2[100]$. We point out, that the two similar permutation symmetries $\hat{\mathbf{P}}_{13}$ and $\hat{\mathbf{P}}_{23}$ of the equivalent equations in cubic systems in Ref. 1 are broken as a consequence of the anisotropy induced by the tetragonal axis. This enables us to distinguish the $D_2[100]{:}B_1$ from the B_2 and B_3 mode. (ii) The B_2 and B_3 modes of a defect with symmetry $D_2[110]$. The B_2 and B_3 modes in (i) and (ii) possess in general different frequencies and can be observed individually. (iii) All twofold-degenerate E modes of a defect. They possess the same frequency and yield exactly the same contribution to the IP. This fact can be used for an identification of E modes, when the degeneracy is lifted by some external perturbation, as, e.g., uniaxial stress.

Dynamical modes of defects with different symmetry properties, which can principally not be distinguished by Raman experiments even if the full set of 21 IP is available, are grouped to sets of so-called representative modes. These sets are listed in Table VI. They are labeled with the representative symmetry O_1 of one mode contained in the set and an arbitrary chosen identifying number for further reference in the first column of Table VI.

In summarizing the results of Tables V and VI, it follows that from a total of 80 possible dynamical modes differing in their symmetry properties, 20 sets of representative modes can possibly be distinguished. This must be compared with 124 possible and 24 representative modes in cubic crystals.[1,7] Comparing with the equivalent Tables V and VI of Ref. 1, the six $C_3[111]$, nine $D_3[111]$, and 30 modes, belonging to the cubic group T, which

TABLE VI. Classification of the 80 dynamical modes which can occur for defects in tetragonal crystals with point groups $O_1' \subset D_{4h}[001]$ into 20 representative modes with point group $O_1 \subset D_4[001]$ which can possibly be distinguished by Raman scattering experiments. The representative modes are given an identifying number for later reference and are labeled with an abbreviated suffix for the complete description of their transformation properties. The meaning becomes obvious by comparison with the preceding Table V.

Representative modes		Number of modes	Dynamical modes
Identifying number	Mode		
1	$C_1 : A$	2	$C_1 : A \quad S_2 : A_g$
2	$C_2[001] : A$	3	$C_2[001] : A \quad C_{1h}(001) : A' \quad C_{2h}[001] : A_g$
3	$C_2[001] : B$	3	$C_2[001] : B \quad C_{1h}(001) : A'' \quad C_{2h}[001] : B_g$
4	$C_2[010] : A$	3	$C_2[010] : A \quad C_{1h}(010) : A' \quad C_{2h}[010] : A_g$
5	$C_2[010] : B$	3	$C_2[010] : B \quad C_{1h}(010) : A'' \quad C_{2h}[010] : B_g$
6	$C_2[110] : A$	3	$C_2[110] : A \quad C_{1h}(110) : A' \quad C_{2h}[110] : A_g$
7	$C_2[110] : B$	3	$C_2[110] : B \quad C_{1h}(110) : A'' \quad C_{2h}[110] : B_g$
8	$D_2[100] : A$	3	$D_2[100] : A \quad C_{2v}(001) : A_1 \quad D_{2h}[001] : A_g$
9	$D_2[100] : B_1$	3	$D_2[100] : B_1 \quad C_{2v}(001) : A_2 \quad D_{2h}[001] : B_{1g}$
10	$D_2[100] : B_2$	6	$D_2[100] : B_2, B_3 \quad C_{2v}(001) : B_1, B_2 \quad D_{2h}[001] : B_{2g}, B_{3g}$
11	$D_2[110] : A$	4	$D_2[110] : A \quad C_{2v}(110) : A_1 \quad D_{2h}[110] : A_g \quad C_{2v}[1\bar{1}0] : A_1$
12	$D_2[110] : B_1$	4	$D_2[110] : B_1 \quad C_{2v}(110) : A_2 \quad D_{2h}[110] : B_{1g} \quad C_{2v}[1\bar{1}0] : B_1$
13	$D_2[110] : B_2$	8	$D_2[110] : B_2, B_3 \quad C_{2v}(110) : B_1, B_2 \quad D_{2h}[110] : B_{2g}, B_{3g}$ $C_{2v}[1\bar{1}0] : A_2, B_2$
14	$C_4[001] : A$	3	$C_4[001] : A \quad S_4[001] : A \quad C_{4h}[001] : A_g$
15	$C_4[001] : B$	3	$C_4[001] : B \quad S_4[001] : B \quad C_{4h}[001] : B_g$
16	$C_4[001] : E$	6	$C_4[001] : E(x'; R_{x'}), E(y'; R_{y'}) \quad S_4[001] : E(x'; R_{x'}), E(y', R_{y'})$ $C_{4h}[001] : E_g^{(1)}, E_g^{(2)}$
17	$D_4[001] : A_1$	4	$D_4[001] : A_1 \quad D_{4h}[001] : A_{1g} \quad D_{2d}[001] : A_1 \quad C_{4v}[001] : A_1$
18	$D_4[001] : B_1$	4	$D_4[001] : B_1 \quad D_{4h}[001] : B_{1g} \quad D_{2d}[001] : B_1 \quad C_{4v}[001] : B_1$
19	$D_4[001] : B_2$	4	$D_4[001] : B_2 \quad D_{4h}[001] : B_{2g} \quad D_{2d}[001] : B_2 \quad C_{4v}[001] : B_2$
20	$D_4[001] : E$	8	$D_4[001] : E(x'; R_{x'}), E(y'; R_{y'}) \quad D_{4h}[001] : E_g^{(1)}, E_g^{(2)}$ $D_{2d}[001] : E(x'; R_{x'}), E(y'; R_{y'}) \quad C_{4v}[001] : E(y'; R_{x'}), E(x'; R_{y'})$
		$\Sigma = 80$	

were classified into seven representative modes in a cubic host, cannot occur in the lower symmetry of tetragonal crystals. On the other hand, the existence of the tetragonal C_4 axis allows us to distinguish between orientations of modes with respect to this axis, introducing six possible modes with $O_1{=}C_2[001]$ and the possible discrimination of the three $D_2[100] : B_1$ modes, forming three new representative modes, which can be distinguished from the others.

It may happen that, due to experimental difficulties, discussed later in Sec. IV B, the analysis of the IP is possible only for one mode of a defect. Then additional limitations occur for the discrimination of the symmetry of the defect. The modes within the following sets cannot be distinguished on the basis of a single-mode analysis even by solving the complete set of IP equations of Table II:

$$\{C_4[001] : A,\ D_4[001] : A\}, \tag{6a}$$

$$\{D_2[110] : B_1,\ D_4[001] : B_1\}, \tag{6b}$$

$$\{D_2[100] : B_1,\ D_4[001] : B_2\}, \tag{6c}$$

$$\{C_4[001] : B,\ D_4[001] : E\}. \tag{6d}$$

This can be proved by an inspection of the explicit expressions of the IP, using the specific Raman tensors of the modes and the O_1 symmetry induced relations between the population numbers, see Sec. III B 2.

In the above discussion of possible distinctions it was not yet considered, whether the equations of Table II can actually be solved, i.e., whether there is a sufficient number of independent IP compared with the number of unknowns $\{N^{(n)}, T_{ij}\}$.

B. Symmetry imposed properties of the Raman IP

1. Properties resulting from partial preferential orientations of the defects

In cubic crystals, due to an averaging of the $h{=}24$ randomly distributed defects only 7 sets out of 25 representative modes can possibly be distinguished, see Table VIII of Ref. 1. Therefore, the distortion of that high symmetry by means of partial preferential orientation is a necessary experimental tool to decide between the transformation properties of defect modes. In tetragonal crystals more information on the Raman tensor of a mode induced by the symmetry O_1 can be extracted from the behavior of the IP in general, even for a random distribution. To achieve this, it is necessary to measure polarized Raman scattering intensities for several orientations of the crystal. There might be experimental difficulties to realize all the necessary scattering configurations. In those cases it may become advantageous to impose some preferential orientation among the defects.

The introduction of the concept of the orientating operator $\hat{\mathbf{F}}$ (Ref. 1) into the BT theory was therefore essential for a complete theoretical description in cubic systems, but there is no such compelling feature in tetragonal systems.

As already stated the number σ of independent population numbers under the orientating action of $\hat{\mathbf{F}}$ is simply the number of right cosets of F_1. Formally, by applying the rules given in Eqs. (12) of Ref. 1 or alternatively by explicit insertion of the constraints on the population numbers $N^{(n)}$ prescribed by the right cosets of F_1 in Table III(a) into the equations for the IP in Table II allows one to find some explicit relations between the 21 IP. If, for a given F_1, there are τ such relations, the number μ_{IP} of independent IP is reduced to $\mu_{\mathrm{IP}} = 21 - \tau$. Using the short IP notations of Eq. (5), these explicit relations induced purely by the symmetry F_1 of the preferential orientation, are given in Table IV. In addition the numbers σ of independent population numbers and of independent IP, μ_{IP}, are listed for each F_1.

When no information on the Raman tensor of the mode is available, the number μ_T of independent tensor elements T_{ij} equals six. Due to the fact that only relative values of the variables $\{T_{ij}, N^{(n)}\}$ and of the IP can be obtained in an experiment, the equations in Table II reduce to a set of $(\mu_{\mathrm{IP}} - 1)$ equations with $N_{\mathrm{var}} = (\mu_T - 1) + (\sigma - 1)$ unknowns. From Table IV we read, that always $(\mu_{\mathrm{IP}} - 1) \geq N_{\mathrm{var}}$, and the equality only holds for $F_1{=}D_4[001]$ and $C_4[001]$. This indicates, that the remaining IP can still not be independent. There must be further implicit constraints among these quantities and it is not obvious, which are the really independent IP.

One example of these implicit constraints can be found by inspection of the explicit equations for the IP in Table II, namely, the relation

$$(q_1 + q_2 + 2r_3)^{\frac{1}{2}} = \frac{(r_1 + r_2)}{(q_3)^{\frac{1}{2}}} \tag{7}$$

which holds generally, if $q_3 \neq 0$.

Further relations may become obvious, if the symmetry O_1 of the mode is explicitly taken into account. This generally simplifies the most general Raman tensor for $O_1{=}C_1$.

2. Properties resulting from the local defect symmetry

The symmetry of a local dynamical mode is reflected in its Raman tensor, see Table V. When the defect symmetry O_1 is raised, the Raman tensor can simplify considerably, i.e., the number of independent tensor elements T_{ij} decreases and more and more elements vanish or become equal when compared with the Raman tensor for $O_1{=}C_1$. Additionally, the number of equivalent orientations v_n of the mode within the crystal increases.

Due to the homomorphic correspondence of the set of transformations $R_n \in O_1$ with the set of orientations v_n obtained from the initial orientation v_1 by $v_n = R_n v_1$, these orientations are essentially equivalent for the defect. It was proved formally in Ref. 1, that the sets of physically equivalent orientations for given defects with symmetry O_1 are obtained by constructing the left cosets

of the subgroup O_1 of the full crystal point group. The left cosets for the representative symmetries O_1 are summarized in Table III(b). As a physically trivial result of this, the population numbers $N^{(n)}$ of the orientations v_n belonging to the same coset are equal.

The simplifications of the IP expressions in Table II due to the simplified Raman tensors combined with the equalities among the population numbers for all representative modes are not worthwhile being tabulated explicitly. The are contained implicitly in Tables VII and IX for the special case F_1=C_1 as discussed in the following section.

3. *Possible behavior types in tetragonal crystals*

The idea of the BT method is not the attempt to solve the IP equations for the occurring unknowns $\{N^{(n)}, T_{ij}^{(1)}\}$, because this will involve some practical problems. (i) The identification of the really independent IP, as discussed in Sec. III B 1. (ii) The expressions in Table II are cubic equations, with a high number of unknowns. (iii) The measurement of polarized intensities in several independent scattering configurations is generally a difficult task in spectroscopy. In addition, (iv) Raman scattering intensities of defects in crystals may become very small, if the concentration of the defects is limited by their solubility in the crystal, reducing experimental precision.

Rather, the idea of the BT method is to try to identify the representative modes on the basis of a direct inspection of simple algebraic relations among their IP induced by the group-theoretical form of the Raman tensor of the symmetry O_1 and the relations among the population numbers induced by the symmetry F_1. In other words, the BT method avoids the cumbersome evaluation of the basic physical quantities $\{N^{(n)}, T_{ij}^{(1)}\}$ and focuses on the related behavior of the IP, which can be more directly obtained in the experiments, as is shown in Sec. IV A below. The complete set of 21 IP together with the algebraic relations between them, is called the *behavior type* of the mode.[1]

In a systematic calculation of the BT for all the possible dynamical modes with all possible preferential orientations it is necessary in a first step to determine the sets of independent population numbers $N^{(n)}$ of the equivalent orientations v_n under the combined influence of the symmetry O_1 of the mode and the preferential orientation with symmetry F_1 by combining the left cosets of O_1 with the right cosets of F_1 according to the rules given in Eqs. (14) and (15) of Ref. 1. In a second step, the explicit forms of the Raman tensors are introduced into the IP expressions.

The occurrence of the following simple types of relations or combinations of them has systematically been investigated:

$$x_i = 0, \tag{8a}$$

$$x_i \leq 0, \tag{8b}$$

$$x_i = cx_j, \tag{8c}$$

$$x_i = c(x_j + x_k), \tag{8d}$$

$$(x_i/x_j) = c(x_k/x_l), \tag{8e}$$

$$(x_i/x_j) = c(x_k/x_l)^{\frac{1}{2}}. \tag{8f}$$

Here, the x_i, x_j, x_k, x_l denote specific IP summarized in Eq. (5), and c is a positive or negative integer of half integer.

As a result of this long but straightforward calculation it was found that 46 different BT are possible in tetragonal crystals. All these possible BT are listed in Table VII. They are given an individual BT number for later reference. The most characteristic IP relations, namely, Eqs. (8a) and (8c) are directly represented in the table. The other more complicated types of Eqs. (8d)–(8f) are listed in the footnote and given an individual label which is referenced in the last column of Table VII.

The first additional BT relation is simply the equivalent of Eq. (7), which is generally valid if $q_3 \neq 0$:

$$(q_1 + q_2 + 2r_3)^{\frac{1}{2}} = \frac{(r_1 + r_2)}{(q_3)^{\frac{1}{2}}}. \tag{7'}$$

If furthermore $q_1 = q_2$ and $r_1 = r_2$ this simplifies to the second additional BT relation:

$$(q_1 + r_3)^{\frac{1}{2}} = \frac{(2r_1)}{(q_3)^{\frac{1}{2}}}. \tag{9}$$

For those modes, where the Raman tensor additionally imposes $T_{11} = T_{22}$, this relation simplifies further to the third additional BT relation:

$$r_1 = (q_1 q_3)^{\frac{1}{2}}. \tag{10}$$

It should be noted, that the two BT pairs nos. (9) and (10) and nos. (15) and (16) differ only within their additional BT relations of the type of Eqs. (8e) and (8f) connecting four IP. All the other BT differ by the more characteristic IP relations of the type of Eqs. (8a) and (8c).

The connection to each of the possible representative modes under all possible symmetries of the orientating operator $\hat{\mathbf{F}}$ is given in Table IX. The entries of that table are the BT numbers defined in Table VII, and the identifying number in the first columm labels the representative modes summarized in Table VI.

The first row of Table IX, which contains the occurring BT for all the possible symmetries F_1 of a preferential orientation for defect symmetry O_1=C_1, contains precisely the F_1-symmetry induced relations among the IP listed explicitly in Table IV. These relations are characteristic for the symmetry F_1 of the externally induced preferential orientation of the defects described by the orientating operator $\hat{\mathbf{F}}$. Because they are valid even for the most general Raman tensor, they must be obeyed for each mode, providing a possibility to check the symmetry of F_1 in the experiment.

In contrast to this, the BT in the first column of Table

TABLE VII. (a) Complete list of the 46 different BT which can occur for the 20 representative modes of defects in tetragonal crystals. They are given an individual BT number for later reference. The main BT relations are directly listed in the table, whereas the additional BT relations between more than two IP are referred to in the last column by identifying numbers referring to part (b) of the table. (b) List of the additional IP relation which occur in the 46 possible different BT for defect modes in tetragonal crystals. The reference number of the relations are those from the last column of part (a) of the table. The numbers of the BT to which the relations belong are also indicated.

(a)

BT number	Main BT relations												Additional BT relations									
	q_1	q_2	q_3	r_1	r_2	r_3	s_1	s_2	s_3	t_1	t_2	t_3	u_1	u_2	u_3	v_1	v_2	v_3	v_4	v_5	v_6	
1	q_1	q_2	q_3	r_1	r_2	r_3	s_1	s_2	s_3	t_1	t_2	t_3	u_1	u_2	u_3	v_1	v_2	v_3	v_4	v_5	v_6	1
2	q_1	q_1	q_3	r_1	r_1	r_3	s_1	s_1	s_3	t_1	t_2	t_3	u_1	u_2	u_3	u_1	v_2	u_2	v_4	v_5	v_5	1, 2, 3, 4, 5, 6, 12, 14
3	q_1	q_1	q_3	r_1	r_1	r_3	s_1	s_1	s_3	t_1	$-t_1$	t_3	u_1	$-u_1$	u_3	v_1	v_2	$-v_1$	$-v_2$	v_5	v_5	1, 2, 7
4	q_1	q_1	q_3	r_1	r_1	r_3	s_1	s_1	s_3	t_1	$-t_1$	t_3	u_1	$-u_1$	u_3	u_1	v_2	$-u_1$	$-v_2$	v_5	v_5	1, 2, 3, 8, 9, 10
5	q_1	q_2	q_3	r_1	r_2	r_3	s_1	s_2	s_3	t_1			u_1			v_1	v_2					1
6	q_1	q_2	q_3	r_1	r_2	r_3	s_1	s_2					u_1	u_2		v_1	v_2	v_3	v_4			1, 4, 11
7	q_1	q_1	q_3	r_1	r_1	r_3	s_1	s_1					u_1	$-u_1$		v_1	v_2	$-v_1$	$-v_2$			1, 2
8	q_1	q_2	q_3	r_1	r_2	r_3	s_1	s_2	s_3			t_3			u_3					v_5	v_6	1
9	q_1	q_1	q_3	r_1	r_1	r_3	s_1	s_1	s_3			t_3			u_3					v_5	v_5	1, 2, 7
10	q_1	q_1	q_3	r_1	r_1	r_3	s_1	s_1	s_3			t_3			u_3					v_5	v_5	1, 2, 3, 6, 14
11	q_1	q_1	q_3	r_1	r_1	q_1	s_1	s_1	s_3	t_1			u_1			u_1	v_2					1, 2, 3, 9, 10, 13
12	q_1	q_2	q_3	r_1	r_2	r_3	s_1	s_2					u_1			v_1	v_2					1
13	q_1	q_1	q_3	r_1	r_1	r_3	s_1	s_1	s_3											v_5	$-v_5$	1, 2
14	q_1	q_2	q_3	r_1	r_2	r_3			s_3						u_3					v_5	v_6	1
15	q_1	q_1	q_3	r_1	r_1	r_3			s_3						u_3					v_5	v_5	1, 2, 6
16	q_1	q_1	q_3	r_1	r_1	r_3			s_3						u_3					v_5	v_5	1, 2, 3, 6, 14
17	q_1	q_1				$-q_1$	s_1	s_1				t_3	u_1	u_2		$-u_1$		$-u_2$				
18	q_1	q_1				$-q_1$	s_1	s_1				t_3	u_1	$-u_1$		$-u_1$		u_1				
19	q_1	q_2	q_3	r_1	r_2	r_3	s_1	s_2	s_3													1
20	q_1	q_1	q_3	r_1	r_1	r_3			s_3											v_5	$-v_5$	1, 2
21	q_1	q_1	q_3	r_1	r_1	r_3	s_1	s_1	s_3													1, 2
22	q_1	q_1	q_3	r_1	r_1	q_1	s_1	s_1	s_3													1, 2, 3
23	q_1	q_2	q_3	r_1	r_2	r_3	s_1	s_2														1
24	q_1	q_1	q_3	r_1	r_1	r_3	s_1	s_1														1, 2
25	q_1	q_2	q_3	r_1	r_2	r_3			s_3													1
26	q_1	q_1	q_3	r_1	r_1	r_3			s_3													1, 2
27	q_1	q_1	q_3	r_1	r_1	q_1			s_3													1, 2, 3
28	q_1	q_1				$-q_1$	s_1	s_1					u_1			$-u_1$						
29	q_1	q_2	q_3	r_1	r_2	r_3																1
30	q_1	q_1	q_3	r_1	r_1	r_3																1, 2
31	q_1	q_1				$-q_1$			s_3											v_5	$-v_5$	
32	q_1	q_1				$-q_1$	s_1	s_1				t_3										
33	q_1	q_1	q_3	r_1	r_1	q_1																1, 2, 3
34							s_1	s_2	s_3	t_1	t_2											
35							s_1	s_1	s_3	t_1	$-t_1$											

TABLE VII. *(Continued).*

BT number	Main BT relations																						Additional BT relations
1	q_1	q_2	q_3	r_1	r_2	r_3	s_1	s_2	s_3	t_1	t_2	t_3	u_1	u_2	u_3	v_1	v_2	v_3	v_4	v_5	v_6		1
36	q_1	q_1				$-q_1$	s_1	s_1															
37							s_1	s_2	s_3	t_1													
38	q_1	q_1				$-q_1$			s_3														
39							s_1	s_2	s_3														
40							s_1	s_2				t_3											
41							s_1	s_1				t_3											
42							s_1	s_1	s_3														
43	q_1	q_1				$-q_1$																	
44							s_1	s_2															
45							s_1	s_1															
46									s_3														

(b)

Reference number	Additional BT relations	Occurrence in BT number
1	$(q_1 + q_2 + 2r_3)^{\frac{1}{2}} = (r_1 + r_2)/(q_3)^{\frac{1}{2}}$ in all BT's when $q_3 \neq 0$	1, 2, 3, 4, 5, 6, 7, 8, 9, 10, 11, 12, 13, 14, 15, 16, 19, 20, 21, 22, 23, 24, 25, 26, 27, 29, 30, 33
2	$(q_1 + r_3)^{\frac{1}{2}} = (2r_1^2/q_3)^{\frac{1}{2}}$ when $q_3 \neq 0$ and $q_1 = q_2$ and $r_1 = r_2$	2, 3, 4, 7, 9, 10, 11, 13, 15, 16, 20, 21, 22, 24, 26, 27, 30, 33
3	$r_1 = (q_1 q_3)^{\frac{1}{2}}$ when $q_3 \neq 0$ and $q_1 = q_2$ and $r_1 = r_2$ and $T_{11} = T_{22}$	2, 4, 10, 11, 16, 22, 27, 33
4	$u_1/u_2 = v_2/v_4$	2, 6
5	$u_1/u_2 = t_1/t_2$	2
6	$q_3/r_1 = u_3/v_5$	2, 10, 15
7	$q_3/r_1 = 2u_3/v_5$	3, 9
8	$u_3/v_5 = r_1/q_1$	4
9	$(s_3/q_3)^{\frac{1}{2}} = t_1/v_2$	4, 11
10	$(s_3/q_1)^{\frac{1}{2}} = t_1/u_1$	4, 11
11	$u_1/u_2 = v_1/v_3$	6
12	$v_5/u_3 = u_2/v_4$	2
13	$q_3/r_1 = v_2/u_1$	11
14	$u_3/v_5 = (q_3/q_1)^{\frac{1}{2}}$	2, 10, 16

IX ($F_1=C_1$) contain those relations among the IP mentioned in Sec. III B 2, which are induced purely by the defect symmetry O_1 and the related form of the Raman tensor. They can be called the minimum BT for a given defect mode, because all the IP relations which they contain must also occur for higher symmetries of F_1.

In the last row at the bottom of Table IX, the number $N_{\rm dis}$ of representative modes is given, which can be distinguished for the indicated orientational symmetry F_1 on the basis of a BT analysis of a single mode of a defect. These numbers are simply the numbers of different BT, which can occur for that symmetry F_1. It turns out, that if in an experiment the preferential symmetry F_1 can be reduced to $F_1=C_2[001]$ or $F_1=C_1$, a single-mode BT analysis provides precisely the same possible discrimination among defect symmetries as it was possible for a complete solution of the IP equations in Table II. Only for the representative modes $\{D_2[110] : B_2$ and $B_3\}$ and those given already by Eqs. (6a)-(6d) the BT become similar, leaving $N_{\rm dis}=16$ distinguishable modes. Even when the random distribution of the defects on their equivalent orientations cannot be influenced in an experiment, i.e., for $F_1=D_4[001]$, and as seen by inspection of Table IX also for $F_1=C_4[001]$, only for three further representative modes the discrimination is hindered, namely,

$$\{C_2[001] : B,\ D_2[100] : B_2,\ D_2[110] : B_2\}. \quad (11)$$

The BT of these modes becomes identical to the BT of the modes $\{C_4[001] : E,\ D_4[001] : E\}$ given in Eq. (6d), which cannot be distinguished at all. This results in $N_{\rm dis}=13$ out of the total of 20 representative modes. It is noted, that for $F_1=D_4[001]$ all A modes of different symmetry O_1 can be distinguished, except for the high symmetric pair $\{C_4[001] : A,\ D_4[001] : A\}$, where both modes yield BT 33. This special BT is unchanged, even when a preferential orientation can be realized and this pair belongs to those modes which cannot be distinguished by single-mode Raman experiments at all, Eq. (6a).

The weak affection of the principal discriminative power for the case of statistical random distribution onto all possible orientations in tetragonal crystals is the consequence of the lower crystal symmetry and the smaller loss of information due to the reduction of the number of equivalent orientations to $h=8$, when compared to cubic crystals with $h=24$. In cubic crystals from a total of 25 representative modes only 15 can possibly be distinguished when F_1 can be lowered to $F_1=C_1$, $C_2[100]$, or $C_2[110]$. This is greatly reduced to $N_{\rm dis}=7$, when no preferential orientation can be realized at all.[1]

4. *Multimode BT analysis of a defect*

The discriminative power of the BT method is enhanced, when more than one mode of the same defect can be detected simultaneously. Except for the $(D_2[110] : B_2, B_3)$ pair, which was already discussed, these modes possess different BT, but they must belong to the same group O_1. These groups of representative modes with the same O_1 are separated by the horizontal lines in Table IX. In favorable cases, all defect orientations with symmetries O_1 can be discriminated.

As an example, the O_1 symmetry of the pair $\{C_4[001] : A,\ D_4[001] : A\}$ can be distinguished even without preferential orientation, if the B mode of the defect can also be detected and identified.

When more than one mode of a defect can be detected, Table VIII may become valuable. For some of the modes there exist additional relations between the IP of different modes of the same defect. These relations are of the form of Eq. (8e), such that the Raman tensor elements cancel out, leaving ratios based on the population numbers, which are equal for the different modes. These relations may yield IP relations of other modes of the defect, which are not directly available from experiment, when the known IP relations of the easily observed mode are substituted therein.

C. Accidental symmetry in a BT: Observed and actual behavior types

A possible complication in the practical performance of a BT analysis of experimental Raman intensity data was already pointed out in Ref. 1. It is necessary to make the following distinction. The IP relations, which are imposed by the actual defect symmetry are called the *actual BT*, in adaptation of the terminology of Ref. 1. These are the ones presented in Tables VII and IX calculated and

TABLE VIII. Relations which exist between the IP of different representative modes of the same defect.

Defect symmetry O_1	Representative modes	IP relations between different modes
$C_2[010]$	4, 5	$\left(\frac{s_1}{s_2}\right)_A = \left(\frac{s_2}{s_1}\right)_B = \frac{N_5+N_6}{N_1+N_2}$
	4, 5	$\left(\frac{u_1}{u_2}\right)_A = \left(\frac{t_1}{t_2}\right)_B = \frac{N_5-N_6}{N_1-N_2}$
$C_2[110]$	6, 7	$\left(\frac{s_1}{t_3}\right)_A = -\left(\frac{s_1}{t_3}\right)_B = -\frac{N_1+N_2+N_3+N_4}{N_1+N_2-N_3-N_4}$
	6, 7	$\left(\frac{u_1}{u_2}\right)_A = \left(\frac{u_1}{u_2}\right)_B = \left(\frac{v_1}{v_3}\right)_A = \left(\frac{v_1}{v_3}\right)_B = \left(\frac{t_1}{t_2}\right)_A = -\frac{N_1-N_2+N_3-N_4}{N_1-N_2-N_3+N_4}$
$D_2[100]$	10, 10	$\left(\frac{s_1}{s_2}\right)_{B_2} = \left(\frac{s_2}{s_1}\right)_{B_3} = \frac{N_5}{N_1}$
$D_2[110]$	13, 14	$\left(\frac{s_1}{t_3}\right)_{B_2} = -\left(\frac{s_1}{t_3}\right)_{B_3} = \frac{N_1+N_3}{N_1-N_3}$

TABLE IX. Summary of the BT which belong to each of the representative modes with symmetry O_1 under the action of an orientating operator $\hat{\mathbf{F}}$ for each possible symmetry F_1. The representative modes are listed in the first column with the abbreviating notation and identifying number introduced in Table VI. The symmetry of $\hat{\mathbf{F}}$ is given in the first row. The entries of the table are the BT numbers defined in Table VII.

O_1	Identifying number	Mode	C_1	$C_2[001]$	$C_2[100]$	$C_2[110]$	$D_2[100]$	$D_2[110]$	$C_4[001]$	$D_4[001]$
C_1	1	A	1	8	5	3	19	9	13	21
$C_2[001]$	2	A	14	14	25	15	25	15	20	26
	3	B	40	40	44	41	44	41	45	45
$C_2[010]$	4	A	6	23	12	7	23	24	24	24
	5	B	34	39	37	35	39	42	42	42
$C_2[110]$	6	A	2	10	11	4	22	10	22	22
	7	B	17	32	28	18	36	32	36	36
$D_2[100]$	8	A	29	29	29	30	29	30	30	30
	9	B_1	46	46	46	46	46	46	46	46
	10	B_2	44	44	44	45	44	45	45	45
$D_2[110]$	11	A	16	16	27	16	27	16	27	27
	12	B_1	43	43	43	43	43	43	43	43
	13	B_2	41	41	45	41	45	41	45	45
$C_4[001]$	14	A	33	33	33	33	33	33	33	33
	15	B	31	31	38	38	38	38	31	38
	16	E	45	45	45	45	45	45	45	45
$D_4[001]$	17	A	33	33	33	33	33	33	33	33
	18	B_1	43	43	43	43	43	43	43	43
	19	B_2	46	46	46	46	46	46	46	46
	20	E	45	45	45	45	45	45	45	45
N_{dis}			16	16	14	14	14	14	13	13

discussed so far.

The result of an analysis of experimental data is what is called the *observed BT*. In general, taking into account experimental uncertainty, the symmetry contained in the observed BT may be higher than the symmetry in the actual BT, because accidental additional IP relations can be pretended.

To give an example, an actual BT shall not require $x_i = x_j$ or $x_i = 0$. But if the Raman tensor elements, which enter the expressions for the IP x_i or x_j happen to be very similar, or very small, respectively, these IP relations might be observed accidentally. From the point of view of the experimentalist, the IP x_i and x_j are equal within experimental uncertainty in the first case and may lie below the detection limit in the second case.

To facilitate a BT analysis concerning these complications, for each possible experimentally *observed BT* the complete set of possible *actual BT* with lower symmetry which may "degenerate" to the observed BT are listed in Table X.

The reverse effect, however, is not possible. That is, the symmetry-induced IP relations of a BT cannot be broken. An example for this are the relations, which stem solely from the symmetry of F_1, see Table IV. It shall be noted, that in the sense of this hierarchy of increasing symmetry contained in a BT, all the possible actual BT of Table VII have been listed in consecutive order using the following scheme of priority.

The order criterion of highest priority for the listing in Table VII was simply the number of IP different from zero. The next weaker criterion was the number of IP which are independent in the sense of the simple BT relation Eq. (8c). The weakest criterion was finally related to the Raman tensor elements contributing to the IP. In the short IP notation, the q_i and r_i are determined from the diagonal tensor elements of $\overline{\mathbf{T}}^{(1)}$ alone. They were assigned a higher priority than the s_i and t_i determined from off-diagonal tensor elements, which were assigned in turn a higher priority than the u_i and v_i. As a consequence of this ordering all possible actual BT for a given observed BT possess a smaller BT number in Table X.

IV. PRACTICAL APPLICATION OF THE METHOD TO TETRAGONAL CRYSTALS

A. Practical sets of optical polarization geometries and limitations due to birefringence

For an application of the BT method it is necessary to obtain as much of the IP as is possible from experimentally measured Raman scattering intensities $I_{\vec{a},\vec{b}}$ under the same condition, i.e., the same experimental detection efficiency k for suitably chosen polarization geometries. From Eqs. (3) and (4) it is clear, that the polarized Raman intensities $I_{\vec{a},\vec{b}}$ depend only on the polarization vectors $\vec{a}$ and $\vec{b}$ of the incident and scattered light waves, respectively, and not on their directions $\vec{k}_{\text{in}}$ and $\vec{k}_{\text{out}}$ of propagation. Therefore, again in adaptation of the terminology of Ref. 1, a pair $(\vec{a}, \vec{b})$ shall be called an *optical geometry pair* (OGP).

Generally the IP are the solutions of a linear system of up to 21 linear independent equations of the type of Eq. (3), where the experimental input data are the $e \in 1, \ldots, 21$ intensities $\left(I_{\vec{a},\vec{b}}\right)_{(e)}$, for the distinctly chosen OGP $\left(\vec{a}_{(e)}, \vec{b}_{(e)}\right)$.

To simplify the evaluation of the IP the following criteria should be fulfilled for OGP's. (i) From the point of view of Eq. (3), the expressions for the scattering intensities shall be as simple as possible. This can be achieved by selecting the $\vec{a}_{(e)}$ and $\vec{b}_{(e)}$ parallel to the axes $x \parallel [100]$, $y \parallel [010]$, and $z \parallel [001]$ of the crystal frame or simply 45° diagonal to them. (ii) Changing to the experimentalist's point of view, only rectangular scattering geometries $\vec{k}_{\text{in}} \perp \vec{k}_{\text{out}}$ are considered. These are commonly preferred to forward or backward scattering geometries ($\vec{k}_{\text{in}} \uparrow\uparrow \vec{k}_{\text{out}}$ or $\vec{k}_{\text{in}} \uparrow\downarrow \vec{k}_{\text{out}}$), because the stray light, originating from surface or Rayleigh scattering, is rejected most efficiently. In addition the signal from the scattering volume can be imaged most efficiently to the entrance slit of the spectrometer. (iii) Additionally, more independent OGP can be realized for $\vec{k}_{\text{in}} \perp \vec{k}_{\text{out}}$ without rotating the sample, i.e., with the same efficiency k. The latter is critically influenced by the orientation of the sample, the quality of the polished sample surfaces and the position of the laser beam. (iv) The sample surfaces shall be $\langle 100 \rangle$, or $\langle 110 \rangle$ planes to simplify the preparation (cutting und polishing) of the crystal for the experiment. The following three sets of OGP were already proposed in Ref. 1 for cubic crystals. The first set is

$$\vec{k}_{\text{in}} \parallel z \perp (001),\ \vec{k}_{\text{out}} \parallel x \perp (100), \tag{12a}$$

the second set is

$$\vec{k}_{\text{in}} \parallel z \perp (001),\ \vec{k}_{\text{out}} \parallel y \perp (010), \tag{12b}$$

and the third set is

$$\vec{k}_{\text{in}} \parallel yz \perp (011),\ \vec{k}_{\text{out}} \parallel x \perp (100). \tag{12c}$$

These scattering geometries are represented schematically in Figs. 1(a)–1(c).

The orientation of the crystal axes must be carefully adjusted within the orthogonal laboratory reference axes, labeled (X, Y, Z). These axes are defined as follows. X is the optical axis of the detection system, usually the monochromator, i.e., $X \parallel \vec{k}_{\text{out}}$. The incident laser beam defines $Z \parallel \vec{k}_{\text{in}}$, which must be adjusted perpendicular to X. The polarization vector $\vec{a}$ of the incident light can then be varied in the X,Y plane, and the polarization $\vec{b}$ of the scattered light in the Y,Z plane.

TABLE X. For each of the BT which may be observed the set of possible actual BT is given. When applying this table to the evaluation of experimental data, only those BT must be considered, which can occur for the symmetry F_1 employed. Observed BT no. 43 can accidentally reduce to nearly all actual BT, therefore only those actual BT to which it can never reduce are given between parentheses.

Observed BT	Possible actual BT	Observed BT	Possible actual BT
1	1	2	1 2
3	1 3	4	1 2 3 4
5	1 5	6	1 6
7	1 3 6 7	8	1 8
9	1 3 4 9	10	1 2 3 4 8 10
11	1 2 5 11	12	1 5 6 12
13	1 8 13	14	1 8 14
15	1 8 9 15	16	1 2 4 8 9 15 16
17	1 17	18	1 3 17 18
19	1 5 8 19	20	1 8 13 14 20
21	1 3 5 9 13 19 21	22	1 2 3 4 5 9 10 11 13 19 21 22
23	1 5 6 8 12 19 23	24	1 3 5 6 7 8 9 12 13 19 21 22 23 24
25	1 5 8 14 19 25	26	1 3 8 9 13 14 15 19 20 21 25 26
27	1 2 3 4 5 8 9 10 11 13 14 15 16 19 20 21 22 25 26 27	28	1 3 5 6 7 12 17 18 28
29	1 5 6 8 12 14 19 23 25 29	30	1 3 5 6 7 8 9 12 13 14 15 19 20 21 23 24 25 26 29 30
31	1 8 13 20 31	32	1 2 3 4 8 9 10 17 18 32
33	1 2 3 4 5 6 7 8 9 10 11 12 13 14 15 16 19 20 21 22 23 24 25 26 27 29 30 33	34	1 34
35	1 2 3 4 34 35	36	1 2 3 4 5 6 7 8 9 10 11 12 13 17 18 19 21 22 23 24 28 32 36
37	1 5 34 37	38	1 2 3 4 5 8 9 10 11 13 14 15 16 19 20 21 22 25 26 27 31 38
39	1 5 8 19 34 37 39	40	1 8 40
41	1 2 3 4 8 9 10 17 18 32 40 41	42	1 2 3 4 5 8 9 10 11 13 19 21 22 34 35 37 39 42
43	(34 35 37 39 40 41 42 44 45 46)	44	1 5 6 8 12 19 23 34 37 39 40 44
45	1 2 3 4 5 6 7 8 9 10 11 12 13 17 18 19 21 22 23 24 28 32 34 35 36 39 40 41 42 44 45	46	1 2 3 4 5 8 9 10 11 13 14 15 16 19 20 21 22 25 26 27 31 34 35 37 38 39 42 46

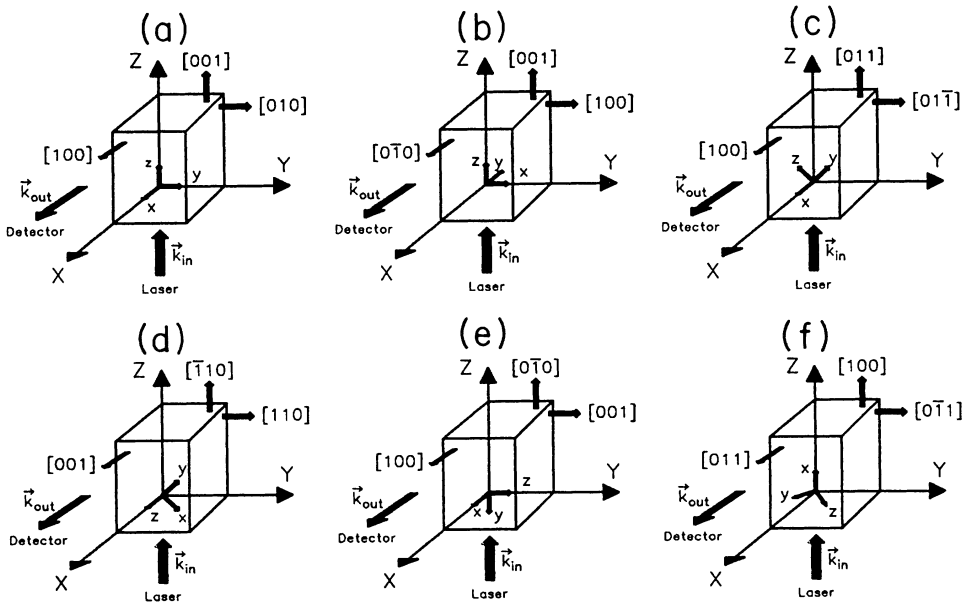

FIG. 1. (a)–(f) Schematic representation of the scattering configurations for the OGP sets introduced in Eqs. (12a)–(12f).

Very often, the experimental set-ups limit the choice of the polarization vectors $\vec{a}$ and $\vec{b}$ to rectangular or 45° diagonal directions, i.e., $\vec{a} \parallel \{X, Y, XY, X\overline{Y}\}$ and $\vec{b} \parallel \{Y, Z, YZ, Y\overline{Z}\}$. This results in 4×4=16 independent scattering intensities, which could be measured within one OGP set, i.e., for one orientation of a cubic crystal. The complete list of these 16 possible OGP and the full expressions of the Raman intensities as a function of the IP for OGP sets 1, 2, and 3 are given in Table XI of Ref. 1.

These three OGP sets are sufficient for use in cubic crystals in the sense that the Raman intensities measured in one of them or a combination of up to all these three sets allows us to distinguish the maximum number N_{dis} of representative modes, see Table XIII of Ref. 1, which can principally be discriminated for any of the possible orientational symmetries F_1 in cubic crystals on the basis of a single mode BT analysis, see Table VIII of Ref. 1. For tetragonal crystals further and/or other OGP sets are necessary to achieve the maximum discrimination, because of two essentially different reasons related to the existence of the unique tetragonal axis.

First, from elementary laws of crystal optics the tetragonal axis destroys the optical isotropy and leads to the effect of birefringence.[9] Tetragonal crystals fall into the category of optically uniaxial crystals, the tetragonal axis being the optical axis of the crystal. In these systems, for each direction $\vec{k}$ of light propagation, only two waves with prescribed directions of polarization can propagate: the ordinary (o) and extraordinary (e) wave. Their polarizations are related to the direction of the optical axis. The plane spanned by the optical axis and the direction $\vec{k}$ of propagation is called the main plane. Then the polarization of the (o) beam is perpendicular, and that of the (e) beam parallel to that plane, in both cases perpendicular to $\vec{k}$. For the special case, when $\vec{k}$ is parallel to the optical axis, all directions perpendicular to $\vec{k}$ are allowed for the polarization.

Generally the birefringence reduces the number of possible OGP which can be measured within one OGP set. The constraints apply for both, the incident and scattered light waves with $\vec{k}_{\text{in}}$ and $\vec{k}_{\text{out}}$, respectively, generally leaving only two possible directions for $\vec{a}$ and $\vec{b}$. This allows only 2×2=4 possible OGP within one OGP set. For the special cases, that either $\vec{k}_{\text{in}}$ or $\vec{k}_{\text{out}}$ is chosen parallel to the optical axis, the experimental set-up limitations mentioned above become important again.

The second demand for further OGP sets arises within the BT method. The lower symmetry of tetragonal crystals compared to cubic systems leads to a higher number of independent IP, which are characteristic for the BT of the representative defect modes.

As an example, consider the case of random distribution of the defects on the equivalent orientations. For cubic systems, at maximum the $\mu_{\text{IP}}=3$ independent IP q, r, s are left, which for the most general Raman tensor $O_1=C_1$ yield BT(cubic) no. 60 ($q_1 = q_2 = q_3 \equiv q$, $r_1 = r_2 = r_3 \equiv r$, $s_1 = s_2 = s_3 \equiv s$), see Tables II, VII, and VIII of Ref. 1 for $F_1=T$ or O. For tetragonal crystals, inspection of the equivalent Tables IV, VII, and IX of this work for $F_1=D_4[001]$ yield $\mu_{\text{IP}}=6$ and BT(tetragonal) no. 21 ($q_1 = q_2 \neq q_3$, $r_1 = r_2 \neq r_3$, $s_1 = s_2 \neq s_3$). The IP, which carry the index 3 in this short IP notation, will generally be different from those with indices 1 and 2. Inspection of Tables VII and IX of this work reveals that the most direct discrimination between the representative modes via a BT analysis involves testing the validity of the following IP relations: $q_3 = 0$, $r_3 = 0$, $r_3 = -q_1$, $s_3 = 0$ and the other relations among the quantities s_1, s_2, and s_3. This emphasizes the need of OGP sets with the most direct access to these specific IP in the sense that the Raman intensities

TABLE XI. Raman scattering intensities $I_{\vec{a},\vec{b}}$, which can be measured together in the six essentially independent OGP sets for uniaxial crystals, given as function of the IP. The scattering configuration is expressed with respect to the laboratory frame (X, Y, Z) defined by $\vec{k}_{\text{in}} \parallel Z$, $\vec{k}_{\text{out}} \parallel X$ and the crystal frame (x, y, z) according to the Porto notation $\vec{k}_{\text{in}}\,(\vec{a}, \vec{b})\,\vec{k}_{\text{out}}$.

Laboratory frame	Crystal frame	$I_{\vec{a},\vec{b}}$
	(a) OGP set 1 : $\vec{k}_{\text{in}} \parallel z, \vec{k}_{\text{out}} \parallel x$	
$Z(Y, Y)X$	$z(y, y)x$	q_2
(Y, Z)	(y, z)	s_1
(X, Z)	(x, z)	s_2
(X, Y)	(x, y)	s_3
(XY, Y)	(xy, y)	$\frac{1}{2}(q_2 + s_3 + 2v_6)$
$(X\overline{Y}, Y)$	$(x\overline{y}, y)$	$\frac{1}{2}(q_2 + s_3 - 2v_6)$
(XY, Z)	(xy, z)	$\frac{1}{2}(s_1 + s_2 + 2t_3)$
$(X\overline{Y}, Z)$	$(x\overline{y}, z)$	$\frac{1}{2}(s_1 + s_2 - 2t_3)$
	(b) OGP set 2 : $\vec{k}_{\text{in}} \parallel z, \vec{k}_{\text{out}} \parallel y$	
$Z(Y, Y)X$	$z(x, x)y$	q_1
(Y, Z)	(x, z)	s_2
(X, Z)	(y, z)	s_1
(X, Y)	(y, x)	s_3
(XY, Y)	$(x\overline{y}, x)$	$\frac{1}{2}(q_1 + s_3 - 2v_5)$
$(X\overline{Y}, Y)$	(xy, x)	$\frac{1}{2}(q_1 + s_3 + 2v_5)$
(XY, Z)	$(x\overline{y}, z)$	$\frac{1}{2}(s_1 + s_2 - 2t_3)$
$(X\overline{Y}, Z)$	(xy, z)	$\frac{1}{2}(s_1 + s_2 + 2t_3)$
	(c) OGP set 3 : $\vec{k}_{\text{in}} \parallel yz, \vec{k}_{\text{out}} \parallel x$	
$Z(Y, Y\overline{Z})X$	$yz(y\overline{z}, z)x$	$\frac{1}{2}(q_3 + s_1 - 2v_2)$
(Y, YZ)	$(y\overline{z}, y)$	$\frac{1}{2}(q_2 + s_1 - 2v_1)$
$(X, Y\overline{Z})$	(x, z)	s_2
(X, YZ)	(x, y)	s_3
	(d) OGP set 4 : $\vec{k}_{\text{in}} \parallel \overline{x}y, \vec{k}_{\text{out}} \parallel z$	
$Z(Y, Y)X$	$\overline{x}y(xy, xy)z$	$\frac{1}{4}(q_1 + q_2) + \frac{1}{2}r_3 + s_3 + (v_5 + v_6)$
(Y, Z)	$(xy, \overline{x}y)$	$\frac{1}{4}(q_1 + q_2) - \frac{1}{2}r_3$
(Y, YZ)	(xy, y)	$\frac{1}{2}(q_2 + s_3 + 2v_6)$
$(Y, Y\overline{Z})$	(xy, x)	$\frac{1}{2}(q_1 + s_3 + 2v_5)$
$Z(X, Y)X$	(z, xy)	$\frac{1}{2}(s_1 + s_2 + 2t_3)$
(X, Z)	$(z, \overline{x}y)$	$\frac{1}{2}(s_1 + s_2 - 2t_3)$
(X, YZ)	(z, y)	s_1
$(X, Y\overline{Z})$	(z, x)	s_2
	(e) OGP set 5 : $\vec{k}_{\text{in}} \parallel \overline{y}, \vec{k}_{\text{out}} \parallel x$	
$Z(Y, Y)X$	$\overline{y}(z, z)x$	q_3
(Y, Z)	(z, y)	s_1
(X, Y)	(x, z)	s_2
(X, Z)	(x, y)	s_3
	(f) OGP set 6 : $\vec{k}_{\text{in}} \parallel x, \vec{k}_{\text{out}} \parallel yz$	
$Z(XY, Y)X$	$x(z, y\overline{z})yz$	$\frac{1}{2}(q_3 + s_1 + 2v_2)$
(XY, Z)	(z, x)	s_2
$(X\overline{Y}, Y)$	$(y, y\overline{z})$	$\frac{1}{2}(q_2 + s_1 - 2v_1)$
$(X\overline{Y}, Z)$	(y, x)	s_3

of Eq. (3) are most simple linear combinations of these characteristic IP.

Apart from the OGP sets 1, 2, and 3 of Ref. 1, three additional OGP sets, 4, 5, and 6, are considered in view of both, the problem of birefringence, and the need to obtain these special IP directly. OGP set 4:

$$\vec{k}_{\text{in}} \parallel \overline{x}y \perp (\overline{1}10),\ \vec{k}_{\text{out}} \parallel z \perp (001), \tag{12d}$$

OGP set 5:

$$\vec{k}_{\text{in}} \parallel \overline{y} \perp (010),\ \vec{k}_{\text{out}} \parallel x \perp (100), \tag{12e}$$

and OGP set 6:

$$\vec{k}_{\text{in}} \parallel x \perp (100),\ \vec{k}_{\text{out}} \parallel yz \perp (011), \tag{12f}$$

are sketched in Figs. 1(d)–1(f). Equivalent OGP sets can be obtained by an exchange of $\vec{k}_{\text{in}}$ and $\vec{k}_{\text{out}}$, which can directly be seen from Eq. (3) using of the fact that $P_{ij\,kl} = P_{kl\,ij}$.

The refractive index of the (e) wave depends on the direction $\vec{k}$ as given by the index ellipsoid.[9] Additional obstacles due to the birefringence occur, when the incident beam is refracted to two directions at the crystal surface. This is suppressed, when geometries are selected with $\vec{k}_{\text{in}}$, $\vec{k}_{\text{out}}$ either parallel or perpendicular to the optical axis. In this respect, OGP set nos. 3 and 6 of Fig. 1 and Table XI, see below, are only recommended, when the birefringence $\Delta n = n_e - n_o$ is very small.

The Raman intensities, which can be measured in these six OGP sets under the constraints of birefringence, are given as a function of the IP in Table XI(a)–(f). The expressions are calculated from Eqs. (3) and (4) for the general symmetry F_1=C_1. The permutation symmetries $P_{ij\,kl} = P_{kl\,ij} = P_{ji\,kl}$ of the IP, which result from the symmetry $T_{ij} = T_{ji}$ of the Raman tensor and the bilinear form of Eq. (4) with respect to the T_{ij}, were used in the derivation. Finally the short IP notation according to Eq. (5) was substituted. The notation of the directions $\vec{k}_{\text{in}}$, $\vec{k}_{\text{out}}$, $\vec{a}$, $\vec{b}$ is the same as that used to label the rotation axes of the transformation matrices R_n in Sec. II. For a specific higher symmetry of F_1, the IP must at least follow the minimum BT for a defect symmetry O_1=C_1. The corresponding IP relations are those explicitly given in the last column of Table IV. They can be used to simplify the expressions of Table XI. In favorable cases, more IP can be solved from the expressions of Table XI.

As an example, the only access to any of the r_i IP, namely, r_3, is possible in OGP set 4. It is much simplified, when $v_5 = v_6 = 0$, because then simply $I_{xy,xy} - I_{xy,x\overline{y}} = r_3 + s_3$. The s_3 IP is directly available in any of the OGP sets 1, 2, 5, or 6.

It is in principle possible to perform intensity measurements in several OGP sets with the aim to determine more of the IP. In this case it is necessary to have at least one OGP, which can be realized in the OGP sets to be combined, in order to evaluate the relative experimental efficiency k. Fortunately, $I_{x,z} = s_2$ can be measured in all of the six proposed OGP sets. By pairwise comparison, at least the two OGP $I_{x,z} = s_2$ and $I_{x,y} = s_3$ or $I_{x,z} = s_2$ and $I_{y,z} = s_1$ are available in all pairs of OGP sets to be combined. When the symmetry of $\hat{\mathbf{F}}$ requires $q_1 = q_2$, then $I_{x,x} = q_1$ and $I_{y,y} = q_2$ can also be used to link OGP sets.

We have checked, that under the constraints of birefringence no other rectangular scattering OGP sets are possible at all, which allow to extract additional IP to the set of these 12 IP:

$$\{q_1, q_2, q_3, r_3, s_1, s_2, s_3, t_3, v_1, v_2, v_5, v_6\}. \tag{13}$$

In Table XII, an overview is given of the individual IP, which can be obtained from measurements within the 6 selected OGP sets or combinations of several of them, for all possible representative symmetries F_1. The F_1-symmetry imposed conditions of Table IV for the IP have explicitly been taken into account. In the second row of Table XII the number $\mu_{\text{uniaxial}}^{\text{rectang}}$ of IP, which can be obtained at maximum for the OGP sets with rectangular scattering geometry under the constraints of birefringence is compared with the number μ_{IP} of independent IP for each symmetry F_1. Furthermore, these $\mu_{\text{uniaxial}}^{\text{rectang}}$ IP are explicitly listed. In the following rows the number of IP and the list of the IP, which can be obtained from measurements within the indicated combination of OGP sets, are tabulated.

It is seen, that in the favorable cases $F_1 = D_2[100]$, $C_4[001]$, or $D_4[001]$ only two OGP sets (namely, OGP sets 4 and 5) must be combined to obtain all the $\mu_{\text{uniaxial}}^{\text{rectang}}$ IP. Three OGP sets, namely, sets {3, 4, 5} or {1, 4, 6} or {1, 4, 5} must be combined for experiments with $F_1 = C_2[100]$ or $C_2[110]$ or $D_2[110]$, respectively, while four OGP sets {1, 2, 4, 6} are necessary for F_1=$C_2[001]$ and even five sets {1, 2, 3, 4, 5} in the case of F_1=C_1.

It is questionable whether sufficient experimental accuracy can be obtained in an experiment in order to obtain the complete BT. Fortunately this is not necessary. The BT method can be most advantageously employed, when for specific preferential orientation symmetries F_1 those OGP sets are selected, which allow us to extract the IP relations, which are characteristic for the BT belonging to the symmetry O_1 of the defect. This is outlined in more detail in Sec. IV B.

We have also considered backscattering configurations $\vec{k}_{\text{in}} \uparrow\downarrow \vec{k}_{\text{out}}$. These geometries are more difficult to perform. However, some additional IP to those in Eq. (13) can be obtained in principle. The relevant OGP sets and the according Raman intensities are

$$\vec{k}_{\text{in}} \parallel \overline{y}z,\ \vec{k}_{\text{out}} \parallel y\overline{z}: \begin{cases} I_{yz,yz} = \frac{1}{4}(q_2 + q_3) + \frac{1}{2}r_1 + s_1 + (v_1 + v_2), \\ I_{yz,x} = \frac{1}{2}(s_2 + s_3 + 2t_1) = I_{x,yz}, \\ I_{x,x} = q_1, \end{cases} \tag{14a}$$

$$\vec{k}_{\text{in}} \parallel xz,\ \vec{k}_{\text{out}} \parallel \overline{(xz)}: \begin{cases} I_{\overline{x}z,\overline{x}z} = \frac{1}{4}(q_1 + q_3) + \frac{1}{2}r_2 + s_2 - (v_3 + v_4), \\ I_{\overline{x}z,y} = \frac{1}{2}(s_1 + s_3 - 2t_2) = I_{y,\overline{x}z}, \\ I_{y,y} = q_2. \end{cases} \tag{14b}$$

The intensities $I_{x,x}$ and $I_{y,y}$ can be used to obtain the relative experimental efficiencies for these OGP sets. No further IP can be obtained in backscattering geometries with uniaxial crystals.

The main systematic experimental errors in polarized Raman intensity measurements result from a deviation of the crystal orientation with respect to the polarization directions. For a complete discussion of this problem we refer to Sec. III E of Ref. 1. Let β_1, β_2, and β_3 denote the small angle misalignment of the crystal with respect to the axes of the laboratory frame of reference obtained by a rotation around the crystals x, y, and z axes. Then a distinction can be made between the cases, when the related error ΔI of the polarized Raman intensity varies

TABLE XII. Independent Raman IP, which can be determined from measurements in one OGP set or from a combined experiment in several OGP sets, for each symmetry F_1 of the orientating operator $\hat{\mathbf{F}}$. The number μ_{IP} of independent IP, the number $\mu_{\mathrm{uniaxial}}^{\mathrm{rectang}}$ of IP, which can be obtained in rectangular scattering geometries, and the explicit list of the nonzero IP are given in the second and third rows of the table for each F_1. The entries of the table are the lists of the specific IP and their number, which can be obtained in the indicated OGP set or combination of sets.

	F_1 symmetry							
OGP sets	C_1	C_2[001]	C_2[100]	C_2[110]	D_2[100]	D_2[110]	C_4[001]	D_4[001]
μ_{IP}	20	12	12	11	8	7	6	5
$\mu_{\mathrm{uniaxial}}^{\mathrm{rectang}}$	12	10	9	8	7	7	6	5
$\mathrm{IP}_{\mathrm{access}}^{\mathrm{rectang}}$	$q_1, q_2, q_3, r_3, s_1, s_2, s_3, t_3, v_1, v_2, v_5, v_6$	$q_1, q_2, q_3, r_3, s_1, s_2, s_3, t_3, v_5, v_6$	$q_1, q_2, q_3, r_3, s_1, s_2, s_3, v_1, v_2$	$q_1, q_3, r_3, s_1, s_3, t_3, v_1, v_5$	$q_1, q_2, q_3, r_3, s_1, s_2, s_3$	$q_1, q_3, r_3, s_1, s_3, t_3, v_5$	$q_1, q_3, r_3, s_1, s_3, v_5$	q_1, q_3, r_3, s_1, s_3
Set 1	6 $q_2, s_1, s_2, s_3, t_3, v_6$	6 $q_2, s_1, s_2, s_3, t_3, v_6$	4 q_2, s_1, s_2, s_3	5 q_1, s_1, s_3, t_3, v_5	4 q_1, s_1, s_2, s_3	5 q_1, s_1, s_3, t_3, v_5	4 q_1, s_1, s_3, v_5	3 q_1, s_1, s_3
Set 2	6 $q_1, s_1, s_2, s_3, t_3, v_5$	6 $q_1, s_1, s_2, s_3, t_3, v_5$	4 q_1, s_1, s_2, s_3	5 q_1, s_1, s_3, t_3, v_5	4 q_2, s_1, s_2, s_3	5 q_1, s_1, s_3, t_3, v_5	4 q_1, s_1, s_3, v_5	3 q_1, s_1, s_3
Set 3	2 s_2, s_3	2 s_2, s_3	2 s_2, s_3	2 s_1, s_3	2 s_2, s_3	2 s_1, s_3	2 s_1, s_3	2 s_1, s_3
Set 4	3 s_1, s_2, t_3	3 s_1, s_2, t_3	2 s_1, s_2	2 s_1, t_3	2 s_1, s_2	2 s_1, t_3	1 s_1	1 s_1
Set 5	4 q_3, s_1, s_2, s_3	4 q_3, s_1, s_2, s_3	4 q_3, s_1, s_2, s_3	3 q_3, s_1, s_3	4 q_3, s_1, s_2, s_3	3 q_3, s_1, s_3	3 q_3, s_1, s_3	3 q_3, s_1, s_3
Set 6	2 s_2, s_3	2 s_2, s_3	2 s_2, s_3	2 s_1, s_3	2 s_2, s_3	2 s_1, s_3	4 q_1, q_3, s_1, s_3	4 q_1, q_3, s_1, s_3
Sets 1 + 2	8 $q_1, q_2, s_1, s_2, s_3, t_3, v_5, v_6$	8 $q_1, q_2, s_1, s_2, s_3, t_3, v_5, v_6$	5 q_1, q_2, s_1, s_2, s_3	5 q_1, s_1, s_3, t_3, v_5	5 q_1, q_2, s_1, s_2, s_3	5 q_1, s_1, s_3, t_3, v_5	4 q_1, s_1, s_3, v_5	3 $q_1, s_1, s_3,$
Sets 1 + 2 + 3	8 $q_1, q_2, s_1, s_2, s_3, t_3, v_5, v_6$	9 $q_1, q_2, q_3, s_1, s_2, s_3, t_3, v_5, v_6$	6 $q_1, q_2, s_1, s_2, s_3, v_1$	5 q_1, s_1, s_3, t_3, v_5	6 $q_1, q_2, q_3, s_1, s_2, s_3$	6 $q_1, q_3, s_1, s_3, t_3, v_5$	5 q_1, q_3, s_1, s_3, v_5	4 q_1, q_3, s_1, s_3
Sets 1 + 2 + 5	9 $q_1, q_2, q_3, s_1, s_2, s_3, t_3, v_5, v_6$	9 $q_1, q_2, q_3, s_1, s_2, s_3, t_3, v_5, v_6$	6 $q_1, q_2, q_3, s_1, s_2, s_3$	6 $q_1, q_3, s_1, s_3, t_3, v_5$	6 $q_1, q_2, q_3 s_1, s_2, s_3$	6 $q_1, q_3, s_1, s_3, t_3, v_5$	5 q_1, q_3, s_1, s_3, v_5	4 q_1, q_3, s_1, s_3
Sets 1 + 4	6 $q_2, s_1, s_2, s_3, t_3, v_6$	6 $q_2, s_1, s_2, s_3, t_3, v_6$	6 $q_1, q_2, r_3 s_1, s_2, s_3$	6 $q_1, r_3, s_1, s_3, t_3, v_5$	6 $q_1, q_2, r_3 s_1, s_2, s_3$	6 $q_1, r_3, s_1, s_3, t_3, v_5$	5 q_1, r_3, s_1, s_3, v_5	4 q_1, r_3, s_1, s_3
Sets 1 + 5	7 $q_2, q_3, s_1, s_2, s_3, t_3, v_6$	7 $q_2, q_3, s_1, s_2, s_3, t_3, v_6$	5 q_2, q_3, s_1, s_2, s_3	6 $q_1, q_3, s_1, s_3, t_3, v_5$	5 q_2, q_3, s_1, s_2, s_3	6 $q_1, q_3, s_1, s_3, t_3, v_5$	5 q_1, q_3, s_1, s_3, v_5	4 q_1, q_3, s_1, s_3
Sets 1 + 6	7 $q_2, s_1, s_2, s_3, t_3, v_1, v_6$	7 $q_2, q_3, s_1, s_2, s_3, t_3, v_6$	5 q_2, s_1, s_2, s_3, v_1	7 $q_1, q_3, s_1, s_3, t_3, v_1, v_5$	5 q_2, q_3, s_1, s_2, s_3	6 $q_1, q_3, s_1, s_3, t_3, v_5$	5 q_1, q_3, s_1, s_3, v_5	4 q_1, q_3, s_1, s_3
Sets 4 + 5	5 q_3, s_1, s_2, s_3, t_3	5 q_3, s_1, s_2, s_3, t_3	7 $q_1, q_2, q_3, r_3 s_1, s_2, s_3$	4 q_3, s_1, s_3, t_3	7 $q_1, q_2, q_3, r_3, s_1, s_2, s_3$	3 q_3, s_1, s_3	6 $q_1, q_3, r_3, s_1, s_3, v_5$	5 $q_1, q_3, r_3 s_1, s_3$
Sets 1 + 2 + 4	9 $q_1, q_2, r_3, s_1, s_2, s_3, t_3, v_5, v_6$	9 $q_1, q_2, r_3, s_1, s_2, s_3, t_3, v_5, v_6$	6 $q_1, q_2, r_3, s_1, s_2, s_3$	6 $q_1, r_3, s_1, s_2, s_3, v_5$	6 $q_1, q_2, r_3 s_1, s_2, s_3$	6 $q_1, r_3, s_1, s_2, s_3, v_5$	5 q_1, r_3, s_1, s_3, v_5	4 q_1, r_3, s_1, s_3
Sets	$1+2+3+4+5$ 9 $q_1, q_2, q_3, r_3, s_1, s_2, s_3, t_3, v_1, v_2, v_5, v_6$	$1+2+4+5$ 10 $q_1, q_2, q_3, r_3, s_1, s_2, s_3, t_3, v_5, v_6$	$3+4+5$ or $4+5+6$ 9 $q_1, q_2, q_3, r_3, s_1, s_2, s_3 v_1, v_2$	$1+4+6$ 8 $q_1, q_3, r_3, s_1, s_3, t_3, v_1, v_5$	$1+4+6$ or $3+4+5$ 7 $q_1, q_2, q_3, r_3 s_1, s_2, s_3$	(1 or 2) + 4 +(5 or 6) 7 $q_1, q_3, r_3, s_1, s_3, t_3, v_5$	$1+4$ +(5 or 6) 6 $q_1, q_3, r_3, s_1, s_3, v_5$	$1+4$ +(5 or 6) 5 q_1, q_3, r_3, s_1, s_3

(i) to first order in the β_i, i.e., $\Delta I \sim \beta_i$ or (ii) to second order, i.e., $\Delta I \sim \beta_i^2$ or $\Delta I \sim \beta_i \beta_j$. The second-order case is of course less critical. In Table XI of Ref. 1 the linear error order (first or second) is indicated for all OGP in sets 1, 2, and 3 for all symmetries of F_1. The results for $F_1 = D_4$, which in tetragonal crystals means no preferential orientation, can be carried over to OGP sets 4–6 introduced in Eqs. (12d)–(12f).

It was discussed already in Sec. III B 3, that in tetragonal crystals a high discriminative power can be obtained even without preferential orientation, $F_1 = D_4$ [001]. Fortunately, all the IP which determine the BT for that case, namely, the q_i, s_i, and r_3, see Table IX, can be obtained with a second-order accuracy. The q_i and s_i are directly available from OGP sets 1, 2, and 5, while r_3 can be derived from set 4. Those OGP, where the Raman intensity varies to first order with the β_i can be advantageously used to correct the alignment of the crystal, when the Raman intensity of the defect mode is monitored without preferential orientation. The details of this procedure are discussed in Ref. 1 in connection with Table XIV of that paper. Carrying over their considerations to tetragonal crystals, the results for the OGP sets 1–6 can most easily be summarized by referring to the laboratory frame of reference X, Y, Z. For those OGP sets, which allow the diagonal pairs of polarization directions under 45° to the laboratory axes, $\vec{a} = XY$ and $X\overline{Y}$ or $\vec{b} = YZ$ and $Y\overline{Z}$, the crystal must be adjusted so to obtain pairwise equalities of the Raman intensities of the defects without preferential orientations applied. In particular it is necessary, that $I_{XY,Y} = I_{X\overline{Y},Y}$ in OGP sets 1 and 2, and that $I_{Y,YZ} = I_{Y,Y\overline{Z}}$ in OGP set 4.

Instead of monitoring the Raman signal of the defect, it might be possible to test these 45° equalities for some phonon or two-phonon excitation lines with appropriate symmetry, e.g., an A-type symmetry. Whether this is possible or not depends on the crystal structure of the host lattice and must be considered individually. This method becomes useful in cases of small Raman signals either due to low defect concentrations or small Raman scattering cross sections T_{ij} of the defect under study.[10]

B. Discriminative power of the BT method in tetragonal crystals

It was discussed already in Sec. III B 3, that the discriminative power of the BT method for defects in tetragonal crystals is higher compared to cubic systems. In order to obtain the maximum discrimination between representative modes indicated by the numbers N_{dis} in Table IX it is in principle required to determine the complete set of IP which define the BT. This number decreases in general, when experiments can only yield part of the IP, e.g., when only one OGP set can be realized. Then it is possible to check only parts of the IP relations. As a result different BT which can occur for a given F_1 can possibly not be distinguished.

By a systematic inspection of the IP, which can be obtained for a specific symmetry of F_1 in each of the OGP sets 1–6, and combinations of them (Table XII), the full set of IP relations, which define the 46 BT possible in tetragonal crystals (Table VII) and the BT, which can principally occur for the 20 possible different representative modes (Table VI), we have determined those representative modes, which cannot be discriminated on the basis of this limited BT analysis. These undistinguishable modes differ in BT relations which cannot be checked within the OGP sets to be combined. On the other hand, in some cases two BT's can be discriminated even though the IP relations by which they differ cannot directly be checked in the experiment. However, the relatively simple form of the expressions for the Raman intensities $I_{\vec{a},\vec{b}}$ in terms of the IP, listed in Table XI, allows us to check characteristic simple, algebraic relations among the $I_{\vec{a},\vec{b}}$ imposed by the BT. In other words discrimination is achieved by checking the behavior of the $I_{\vec{a},\vec{b}}$, which are the directly measurable quantities, induced by the BT of the IP.

The result of this long but straightforward consideration is presented in Table XIII. The sets of undistinguishable representative modes are given between parentheses for all OGP sets and useful combination of several sets. The representative modes are labeled with their identifying number given in Table VI.

Although OGP sets 1 and 2 yield higher numbers of IP for each symmetry F_1, the other sets offer a comparable, in special cases even higher number of sets of distinguishable modes. This is possible, because in many cases the BT relations among the IP imply certain relations among the Raman intensities $I_{\vec{a},\vec{b}}$ of Table XI, which can be checked in the experiment. This allows characteristic distinctions without solving the expressions of Table XI for the IP, which is not possible, when some of the IP occurring in the intensity expressions are not known.

A good example for this is a case appearing in OGP set 6 for F_1=C_1 or F_1=C_2[001]. For that case, the set of modes {3, 10}={C_2[001] : B, D_2[100] : B_2}, see Table VI, which possess {BT 40, BT 44}, respectively, can be distinguished from the set of modes {13, 16, 20}={D_2[110] : B_2, C_4[001] : E, D_4[001] : E}, which possess {BT 41, BT 45, BT 45}, respectively. The characteristic difference between the sets {BT 40, BT 44} and {BT 41, BT 45} is the relation $s_1 = s_2$, which must be obeyed in the BT within the first set but not in the second set. These two IP cannot be obtained in OGP set 6. However, the characteristic equality can principally be tested when the ratios $I_{z,y\overline{z}}/I_{z,x} = \frac{1}{2}(q_3 + s_1 + 2v_2)/(s_2)$ or alternatively $I_{y,y\overline{z}}/I_{z,x} = \frac{1}{2}(q_2 + s_1 - 2v_1)/(s_2)$ are equal to $\frac{1}{2}$, or not. Note, that for the given symmetry F_1 $v_1 = v_2 = 0$ and that $q_2 = q_3 = 0$ for the BT of the modes to be distinguished.

Having established Table XIII, it turns out furthermore, that at most two OGP sets need to be combined in order to obtain the maximum possible distinction. Namely, OGP sets 1 and 4, when combined for F_1=C_2[001], D_2[001], and D_4[001], or OGP sets 4 and 6, when combined for F_1=C_1, C_2[001], C_2[100], D_2[001], C_4[001], or D_4[001], allow the maximum distinction sug-

gested by Table IX. The sets of modes $\{1, 6\}=\{C_1 : A, C_2[110] : A\}$ and $\{2, 11\}=\{C_2[001] : A, D_2[110] : A\}$ cannot be distinguished at all for $F_1=C_2[110]$ or $F_1=D_2[110]$, because according to Tables VII and IX the difference in the related BT necessitates a determination of the u_i and r_1 IP, which cannot be determined from rectangular scattering geometries.

When the additional discrimination, which can be obtained for a combination of two OGP sets, shall be established, it is not sufficient to look simply whether modes, which belong to a set of nondistinguishable modes for one OGP set, belong to different sets of the other OGP set, although such observations facilitate the establishment enormously. It may happen, that two modes cannot be distinguished in both OGP sets either, when regarded individually. But by a determination of the relative efficiencies k and certain IP relations obtainable in one OGP set it may become possible to discriminate the two modes, when the obtained IP relations are used to check characteristic relations for the Raman intensities in the other OGP set.

An example for this appears for the case of a combination of OGP sets 1 and 4. For $F_1=D_4[001]$ the modes $\{2, 15\}=\{C_2[001] : A, C_4[001] : B\}$, which possess {BT 26, BT 38} cannot be distinguished in either of the OGP sets 1 and 4 alone. The characteristic difference in the IP relations of these two competing modes is that $r_3 = -q_1$ is additionally implied by BT 38 compared to BT 26. When this is inserted into the expressions for the Raman intensities for OGP set 4 in Table XI, one obtains $I_{xy,xy} = s_3$ and $I_{xy,x\bar{y}} = q_1$. Thus for BT 38 the experimental ratio $I_{xy,xy}/I_{xy,x\bar{y}}$ measured in OGP set 4 must be the same as $s_3/q_1 = I_{xy}/I_{xx}$ measured in OGP set 1. If this relation is not verified in the experiment, BT 38 can be ruled out.

We want to point out, that the problems of accidental additional IP relations, which was discussed in Sec. III C, has not been taken into account when establishing Table XIII. As shown in the example given above, accidental additional relations may also arise among the Raman intensities $I_{\vec{a},\vec{b}}$ of Table XI.

C. Realization of partially orientated defect ensembles in tetragonal systems

Finally we want to discuss possible useful applications of the complete formalism of preferential orientation for defects in tetragonal systems. In contrast to cubic crystals, where the concept of partial preferential orienta-

TABLE XIII. The sets of representative modes, which cannot be distinguished from each other on the basis of a single mode BT analysis for selected suitable OGP sets or combinations of them, for all possible symmetries F_1 of the orientating operator $\hat{\mathbf{F}}$. The number $N_{\text{dis}}^{\text{act}}$ of sets of modes, which actually can be discriminated, is compared with the number N_{dis} of modes, see Table IX, which can principally be distinguished for each F_1.

OGP sets	F_1 symmetry	$N_{\text{dis}}^{\text{act}}$	N_{dis}	Distinguishable sets of representative modes
Set 1 or 2	C_1, or $C_2[001]$	12	16	(1)(2,11,15)(3)(4)(5)(6)(7)(8,12,14,17,18)(9,19)(10)(13)(16,20)
	$C_2[100]$, or $D_2[100]$	10	14	(1)(2,11,15)(3,10)(4)(5)(6)(7)(8,12,14,17,18)(9,19)(13,16,20)
	$C_2[110]$, or $D_2[110]$	10	14	(1,6)(2,11)(3,13)(4)(5)(7)(8,12,14,17,18)(9,19)(10,16,20)(15)
	$C_4[001]$	9	13	(1)(2,15)(3,10,13,16,20)(4,7)(5)(6)(8,12,14,17,18)(9,19)(11)
	$D_4[001]$	7	13	(1,6)(2,11,15)(3,10,13,16,20)(4,7)(5)(8,12,14,17,18)(9,19)
Set 3	all F_1	4		(1, 5, 6) (2, 9, 11, 15, 19) (3, 4, 7, 10, 13, 16, 20) (8, 12, 14, 17, 18)
Set 4	C_1	13	16	(1)(2,8,15)(3)(4)(5,10)(6)(7)(9,19)(11)(12,18)(13)(14,17)(16,20)
	$C_2[001]$	15	16	(1)(2,8)(3)(4)(5)(6)(7)(9,19)(10)(11)(12,18)(13)(14,17)(15)(16,20)
	$C_2[100]$	10	14	(1,4)(2,8)(3,10)(5)(6)(7)(9,11,14,17,19)(12,18)(13,16,20)(15)
	$C_2[110]$, or $D_2[110]$	9	14	(1,6)(2,8,11,15)(3,13)(4)(5)(7)(9,14,17,19)(10,16,20)(12,18)(16,20)
	$D_2[100]$	9	14	(1,4)(2,8)(3,10)(5)(6)(7,12,18)(9,11,14,17,19)(13,16,20)(15)
	$C_4[001]$	8	13	(1,4)(2,8,15)(3,10,13,16,20)(5)(6)(7)(9,11,14,17,19)(12,18)
	$D_4[001]$	9	13	(1,4)(2,8,15)(3,5,10,13,16,20)(6)(7)(9,19)(11)(12,18)(14,17)
Set 5	C_1 or $C_2[001]$	10	16	(1)(2,11)(3,10)(4)(5)(6)(7,13,16,20)(8,14,17)(9,15,19)(12,18)
	$C_2[100]$ or $D_2[100]$	10	14	
	$C_2[110]$ or $D_2[110]$	8	14	(1,6)(2,11)(3,7,10,13,16,20)(4)(5)(8,14,17)(9,15,19)(12,18)
	$C_4[001]$ or $D_4[001]$	8	13	
Set 6	C_1 or $C_2[001]$	11	16	(1,6)(2,11)(3,10)(4)(5)(7)(8,14,17)(9,19)(12,18)(13,16,20)(15)
	$C_2[100]$ or $D_2[100]$	11	14	
	$C_2[110]$ or $D_2[110]$	10	14	(1,6)(2,11)(3,10,13,16,20)(4)(5)(7)(8,14,17)(9,19)(12,18)(15)
	$C_4[001]$ or $D_4[001]$	10	13	
Set 1 + 4	C_1	15	16	(1)(2,15)(3)(4)(5)(6)(7)(8)(9,19)(10)(11)(12,18)(13)(14,17)(16,20)
	$C_2[001]$	16	16	(1)(2)(3)(4)(5)(6)(7)(8)(9,19)(10)(11)(12,18)(13)(14,17)(15)(16,20)
	$C_2[100]$ or $D_2[100]$	14	14	(1)(2)(3,10)(4)(5)(6)(7)(8)(9,19)(11)(12,18)(13,16,20)(14,17)(15)
	$C_2[110]$ or $D_2[110]$	12	14	(1,6)(2,11)(3,13)(4)(5)(7)(8)(9,19)(10,16,20)(12,18)(14,17)(15)
	$C_4[001]$	12	13	(1)(2,15)(3,10,13,16,20)(4)(5)(6)(7)(8)(9,19)(11)(12,18)(14,17)
	$D_4[001]$	13	13	(1)(2)(3,10,13,16,20)(4)(5)(6)(7)(8)(9,19)(11)(12,18)(14,17)(15)
Set 1 + 5	C_1 or $C_2[001]$	14	16	(1)(2,11)(3)(4)(5)(6)(7)(8,14,17)(9,19)(10)(12,18)(13)(15)(16,20)
	$C_2[100]$ or $D_2[100]$	12	14	(1)(2,11)(3,10)(4)(5)(6)(7)(8,14,17)(9,19)(12,18)(13,16,20)(15)
	$C_2[110]$ or $D_2[110]$	11	14	(1,6)(2,11)(3,13)(4)(5)(7)(8,14,17)(9,19)(10,16,20)(12,18)(15)
	$C_4[001]$	12	13	(1)(2)(3,10,13,16,20)(4)(5)(6)(7)(8,14,17)(9,19)(11)(12,18)(15)
	$D_4[001]$	10	13	(1,6)(2,11)(3,10,13,16,20)(4)(5)(7)(8,14,17)(9,19)(12,18)(15)
Set 4 + 5	C_1 or $C_2[001]$	16	16	(1)(2)(3)(4)(5)(6)(7)(8)(9,19)(10)(11)(12,18)(13)(14,17)(15)(16,20)
	$C_2[100]$ or $D_2[100]$	14	14	(1)(2)(3,10)(4)(5)(6)(7)(8)(9,19)(11)(12,18)(13,16,20)(14,17)(15)
	$C_2[110]$ or $D_2[110]$	12	14	(1,6)(2,11)(3,13)(4)(5)(7)(8)(9,19)(10,16,20)(12,18)(14,17)(15)
	$C_4[001]$ or $D_4[001]$	13	13	(1)(2)(3,10,13,16,20)(4)(5)(6)(7)(8)(9,19)(11)(12,18)(14,17)(15)

tion is essential in order to increase the relatively small number $N_{dis}=7$, for random orientation of the defects, compared to 25 distinguishable modes,[1] very much information of the symmetry O_1 of the defect inherent in the Raman tensor is preserved and reflected in characteristic IP relations even for random orientation of defects in tetragonal crystals, see Sec. III B 3.

According to the recent review[7] the only physical effect inducing a preferential orientation of the defects among the possible orientations, which was investigated so far using the complete formalism of the BT method for cubic crystals, is polarized optical (uv) bleaching, applied to the $H_i^0(I^-)$ center in RbCl,[2] which gave the initiative for the development of the BT theory.[1] The formalism of treating preferential orientations is applied in a straightforward way to tetragonal systems in this paper. The considerations for F_1 lower than $D_4[001]$ in the tables of this work become relevant for application, when preferentially orientated defects in cubic crystals are investigated under the additional influence of a strong externally sustained field with vector character, e.g., a static electric field or uniaxial stress, which might affect the cubic symmetry of the crystal to become tetragonal. Another application occurs, when anisotropic defects in tetragonal systems, which are able to continually reorient, either by thermal activation or tunneling process, can be influenced by a weak external field, which influences the population numbers $N^{(n)}$ of the individual orientations, but not the crystal symmetry. However, to our knowledge such systems have not yet been investigated.

V. CONCLUDING REMARKS

In this work we have systematically extended the behavior-type method for the interpretation of polarized Raman scattering intensities to point defect modes in tetragonal crystals. Although the number of possible independent polarized scattering geometries is strongly reduced by the effect of birefringence as a consequence of the loss of optical isotropy, this does not affect the discriminative power of the method for the proposed scattering geometries, making the method a powerful tool for investigations also in tetragonal systems.

We were stimulated to extend the method to tetragonal crystals from Raman investigations of hydrogen impurities in oxidic crystals. The hydrogen performs the well-known OH-stretching vibration when bound to the oxygen atoms of the lattice. For example in the perovskites $SrTiO_3$ and $KTaO_3$, three competing atomistic models, which differ in the local symmetry O_1, were proposed for the incorporation of hydrogen.[11] Namely, these are the cube axis (CA) model, where the hydrogen is vibrating toward the next-nearest-neighbor oxygen atoms along the cubic ⟨100⟩ axes, the octahedron edge (OE) model, where the hydrogen vibrates along the O–O bonds along the edges of the oxygen octahedra, and the cube face (CF) model, where the hydrogen is placed on the (100) faces between the O^{2-} and the Sr^{2+} or K^+ ion. In the cubic phase the O-H dipoles are isotropically distributed and thus the three models cannot be distinguished by polarized ir absorption measurements. However, polarized Raman measurements analyzed with the BT method for cubic crystals allow us to exclude the CA model, while the OE and CF models cannot be distinguished because of an accidental degeneracy of the related BT for random distribution.[12] The degeneracy of the BT could be lifted, if a preferential orientation with a symmetry F_1 lower than $D_4[001]$ could be realized. However, a reorientational behavior of the OH dipoles, which is known to occur in the alkali halides, has never been observed in oxidic materials under study. Below $T_c = 108$ K, $SrTiO_3$ becomes a tetragonal crystal. For each site proposed by the OE model, there is one corresponding site in the CF model with the same direction of the OH dipole. Hence, these two models are undistinguishable by polarized ir absorption, but the application of the BT method for tetragonal systems to this problem shows, that the remaining competing OE and CF models can principally be distinguished even for random distribution of the hydrogen impurities by polarized Raman experiments, and helped to find the suitable OGP set for an experimental decision.[12] Recent results from the tetragonal phase of $SrTiO_3$ exclude the CF model.[13]

An extension of the BT method to trigonal systems, like $LiTaO_3$ or $LiNbO_3$ crystals, which are of importance in many applications like electrooptical devices or wave guides is also in progress, again for the investigation of OH modes. The tables to be compiled will show, whether polarized Raman scattering can yield additional information to that obtained so far from ir absorption studies also for these systems.

ACKNOWLEDGMENT

This work was supported by the Deutsche Forschungsgemeinschaft, SFB 225.

[1] J. F. Zhou, E. Goovaerts, and D. Schoemaker, Phys. Rev. B **29**, 5509 (1984).
[2] J. F. Zhou, E. Goovaerts, and D. Schoemaker, Phys. Rev. B **29**, 5533 (1984).
[3] W. Joosen, J. F. Zhou, E. Goovaerts, and D. Schoemaker, Phys. Rev. B **31**, 6709 (1985).
[4] W. Joosen, E. Goovaerts, and D. Schoemaker, Phys. Rev. B **34**, 1273 (1986).
[5] W. Joosen, E. Goovaerts, and D. Schoemaker, Phys. Rev. B **32**, 6748 (1985).
[6] M. Leblans, Ph.D. thesis, University of Antwerp, 1990.
[7] W. Joosen and D. Schoemaker, J. Phys. Chem. Solids **51**, 821 (1990).
[8] R. Claus, L. Merten, and J. Brandmüller, *Light Scattering by Phonon-Polaritons*, Springer Tracts in Modern Physics, Vol. 75 (Springer, New York, 1975).
[9] M. Born and E. Wolf, *Principles of Optics*, 5th ed. (Pergamon, New York, 1975).
[10] S. Klauer and M. Wöhlecke, Meas. Sci. Technol. (to be published).
[11] G. Weber, S. Kapphan, and M.Wöhlecke, Phys. Rev. B **34**, 8406 (1986).
[12] S. Klauer and M.Wöhlecke, Ferroelectrics **125**, 385 (1992); **125**, 811 (1992).
[13] S. Klauer and M. Wöhlecke, Phys. Rev. Lett. **68**, 3212 (1992).